View Article Online / Journal Homepage / Table of Contents for this issue
Dynamic Article Links

ChemComm

Cite this: *Chem. Commun.*, 2011, **47**, 3351–3370

www.rsc.org/chemcomm

FEATURE ARTICLE

Porous metal–organic frameworks as platforms for functional applications

Hai-Long Jiang and Qiang Xu*

Received 7th December 2010, Accepted 21st December 2010
DOI: 10.1039/c0cc05419d

Metal–organic frameworks (MOFs), also known as coordination polymers, have emerged as a new class of crystalline porous materials, which are constructed from metal ions or metal ion clusters and bridging organic linkers. MOFs have tunable pores and functionalities, and usually exhibit very high surface areas. The potential applications of porous MOFs cover a broad range of fields and most of their applications are related to pore sizes, shapes and structures/environments. In this *feature article*, we provide an overview of the recent developments of porous MOFs as platforms in the functional applications of sorption and separation, heterogeneous catalysis, as supports/host matrices for metal nanoparticles, and as templates/nanoreactors for new material preparation.

Downloaded by University of Science and Technology of China on 07/05/2013 04:06:21.
Published on 02 February 2011 on http://pubs.rsc.org | doi:10.1039/C0CC05419D

1. Introduction

Metal–organic frameworks (MOFs), also known as coordination polymers, were regarded to have first been developed around 20 years before.[1] They have infinite crystalline lattices which generally involve two main components of inorganic vertices (metal ions or clusters) and organic linkers/struts. The two main components are connected to each other by coordination bonds, together with other intermolecular interactions, to afford a network having definite topology with pores usually occupied by solvent molecules (Fig. 1).

Emerging as a new class of porous materials, MOFs have attracted tremendous attention in recent years, as can be seen from the rapidly increasing publications devoted to this field.[2] In contrast to the preferred new structure explorations and investigations in early stage, the development of multi-functional applications of MOFs have attracted more scientific interest in recent decades.[2] Due to the close correlation between MOF structures and their potential properties, the "real design" of desirable structures with expected properties becomes very important and attractive although it is still a very challenging issue. Generally speaking, most of the

National Institute of Advanced Industrial Science and Technology (AIST), Ikeda, Osaka 563-8577, Japan. E-mail: q.xu@aist.go.jp; Fax: +81-72-751-7942; Tel: +81-72-751-9562

Hai-Long Jiang

Hai-Long Jiang was born in Anhui, P. R. China in 1981. He received his PhD degree from Fujian Institute of Research on the Structure of Matter, Chinese Academy of Sciences (CAS) in 2008 under the supervision of Prof. Jiang-Gao Mao, working on the syntheses, structures and properties of metal selenites and tellurites. He then joined Prof. Qiang Xu's group at AIST as a postdoctoral fellow and became a JSPS (Japan Society for the Promotion of Science) fellow in 2009. He is currently interested in the development of porous materials and nanostructured materials for applications in catalysis, separation, sensing and hydrogen storage.

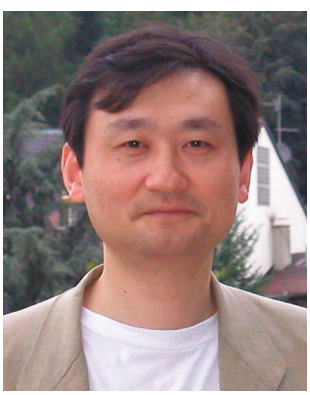

Qiang Xu

Qiang Xu received his PhD degree in Physical Chemistry in 1994 at Osaka University, Japan. After one year working as a postdoctoral fellow at Osaka University, he started his career as a Research Scientist at Osaka National Research Institute in 1995. Currently, he is a Senior Research Scientist at the National Institute of Advanced Industrial Science and Technology (AIST, Japan), adjunct professor at Kobe University, and fellow of the Royal Society of Chemistry (FRSC). His research interests include porous materials and nanostructured materials and related functional applications, especially for clean energy. He has published more than 200 papers in refereed journals.

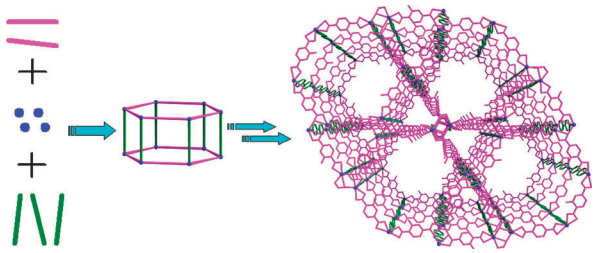

Fig. 1 A general scheme of MOF synthesis.

Downloaded by University of Science and Technology of China on 07/05/2013 04:06:21.
Published on 02 February 2011 on http://pubs.rsc.org | doi:10.1039/C0CC05419D

functional properties of MOFs are dominated by their pores. Therefore, to construct MOFs with suitable pore sizes, shapes and environments is of great interest and importance for their functional applications. Porous MOFs generally have microporous (<2 nm) characters whereas the pore sizes could be tuned from several angstroms to several nanometers by typically controlling the length of the rigid organic ligands or by controlling the interpenetration, *etc*.[3] Moreover, the pore walls and environments can be modified/functionalized by specific ligand design or postsynthetic modification (PSM).[4] The extensive modulations of pore sizes and framework structures of MOFs endow them an incredibly high surface area (>3000 m^2 g^{-1}, and the latest Lagmiur surface area record of over 10 000 m^2 g^{-1}).[5] These unique characteristics of MOFs set them apart from other traditional porous materials. Zeolites and mesoporous silica are usually crystalline but fully inorganic and thus lack synthetic flexibility and structural diversity/tailorability, and porous carbon materials and aerogels are almost amorphous or partially ordered.

Porous MOFs were found to have extremely plentiful structures and topologies,[6] and have been developed as multifunctional materials to display versatile excellent physical properties, such as, magnetism,[7] fluorescence,[8] catalysis,[9] gas storage and separation,[10] hosting guest molecules or nanoparticles (NPs) or as nanoreactors,[11] thin films,[12] sensing or recognition,[3g,13a] proton conduction,[13b–e] drug delivery,[14] and so on. Considering the available reviews on MOFs (especially the MOF themed issue of *Chem. Soc. Rev.* in 2009),[2,15] in this feature article, we focus on the recent developments concerning the following four newly emerging functional applications: sorption and separation, heterogeneous catalysis (mainly, gas-phase), as supports/host matrices for small metal NPs, and as templates/nanoreactors for new material syntheses. Although still in their infancy, the currently available results have unambiguously demonstrated that a bright future is foreseen for the development of porous MOFs in these aspects.

2. Sorption and separation

2.1 Gas storage and separation

2.1.1 Gas storage. Energy consumption all over the world is dramatically increasing due to the rising standards of living and a growing population. Meanwhile, the increasing atmospheric level of carbon dioxide irreparably damages the global ecosystem. These challenges motivate more research into clean energy and environment protecting fields. One of the most extensively studied applications of porous MOFs is their storage and separation capabilities for small molecules, such as, H_2, CO_2, CH_4, *etc*. Since the first report of hydrogen adsorption on a porous MOF in 2003, over 200 porous MOFs have been examined for H_2 storage applications.[16] Recently, we constructed an eight-connected mesoporous MOF and its amino-functionalized analog, which also exhibit relatively high values of 2.08 and 2.31 wt% of H_2 at 1.0 atm and 77 K, respectively. It has been found that the functionalization of amines leads to the effective use of the central space for the adsorption of small molecules, and thus results in the enhancement of adsorption capacity.[17] With great efforts, the hydrogen storage capability of MOFs at 77 K is very promising.[18] A total uptake of 10.0 wt% H_2 for MOF-5 at 77 K and 100 bar, corresponding to a record volumetric storage density of 66 g L^{-1}.[18a] In addition, Yaghi and coworkers proposed MOF-177 as a benchmark adsorber, which possesses a surface excess weight percentage of H_2 uptake of 7.5 wt% at 70 bar and an absolute adsorbed amount of 11 wt%.[18b] Afterward, Saha *et al*. achieved the highest hydrogen adsorption capacity of MOF-177 (11.0 wt% excess, 19.67 wt% absolute adsorption) among all physical adsorbents at 77 K and 100 bar in 2008.[18c] Unfortunately, the relatively low hydrogen uptake was achieved at room temperature due to the interaction energy of just several (typically 3–10) kJ mol^{-1} between the MOF framework and H_2 molecules whereas the desired binding energy is ~20 kJ mol^{-1} for room temperature H_2 storage.[10c]

Besides pure MOFs, several approaches on doped/modified MOFs have been developed to improve hydrogen storage capacity of MOFs. The spillover mechanism[19] proposed by Li *et al*. has been adopted to prepare Pt/Pd NP doped MOFs for enhanced enhanced hydrogen storage applications.[20] Sabo *et al*. reported that MOF-5 impregnated with 1 wt% Pd results in an increase of reversible hydrogen storage of up to 1.86 wt% at 1 bar at 77 K.[20a] The H_2 storage features of Pt@MOF-177 has been investigated in a gravimetric fashion (magnetic suspension balance) to show almost 2.5 wt% in the first cycle at 25 °C and 144 bar whereas it sharply decreases down to 0.5 wt% in consecutive cycles. It is found that the H_2 uptake is not completely reversible in the first cycle, but it becomes completely reversible in the second and third cycles after the drop in H_2 uptake. The MOF-177 framework remains during the spillover process from PXRD examinations. The authors proposed that the loss in uptake was attributed to the formation of palladium hydrides, which were not desorbed at room temperature.[20b] Cheon and Suh have fabricated $Pd@(SNU\text{-}3)^{0.54+}(NO_3^-)_{0.54}$ (SNU-3 = $Zn_3(ntb)_2$, ntb = 4,4′,4″-nitrilotrisbenzoate) and found that the Pd loading amount was correlated with H_2 uptake capacity, where 3 wt% content was shown to be the optimal value for the best H_2 storage. Results indicate that the H_2 storage capacity of 3 wt% $Pd@(SNU\text{-}3)^{0.54+}(NO_3^-)_{0.54}$ is 1.48 wt% compared to 1.03 wt% for SNU-3 although the surface area significantly decreases upon Pd loading. At 25 °C and 95 bar, the excess H_2 adsorption capacity of a Pd-loaded sample is 0.30 wt%, 2.3 times greater than that of SNU-3 (0.13 wt%). In addition, the studies of H_2 adsorption at isosteric heats indicate that the enhanced H_2 adsorption in the Pd-loaded sample is not related to the isosteric heat of H_2 adsorption, but associated with the spillover effect of Pd NPs that dissociate H_2 molecules.[20c]

 This journal is © The Royal Society of Chemistry 2011

Downloaded by University of Science and Technology of China on 07/05/2013 04:06:21.
Published on 02 February 2011 on http://pubs.rsc.org | doi:10.1039/C0CC05419D

Pd@MIL-100(Al) with ~2 nm Pd NPs was reported to have significant changes in H_2 sorption properties compared to pristine MIL-100. The loss of excess hydrogen storage at low temperature can be attributed to the decrease of the specific surface area and pore volume after Pd loading. At room temperature, the hydrogen uptake of Pd@MIL-100 is almost twice that of MIL-100. The authors proposed that the results were correlated with both Pd hydride formation and the spillover mechanism.[20d] Alternatively, both theoretical[21a–c] and experimental[21d–f] results have shown that doping the MOF framework with electropositive alkali metal cations, especially Li^+, can substantially enhance H_2 uptake. Mulfort and Hupp have prepared a ~5 mol% Li^+ doped Zn-MOF, which presented nearly double (1.63 wt%) of H_2 capacity with greater isosteric heat of adsorption compared with that of the pristine MOF (0.93 wt%).[21d] They have also found that H_2 binding intensity with Zn-MOF decreases as $Li^+ > Na^+ > K^+$ whereas H_2 uptake increases in the opposite order. The authors attributed the behavior to structural changes along with framework reduction.[21e] Yang *et al.* have also reported an enhanced H_2 uptake coupled to an increase in the isosteric heat of adsorption and elimination of hysteretic H_2 adsorption upon exchanging piperazinium dications in MOF pores with Li^+.[21f] In addition, supercritical processing (also known as freeze drying) and PSM and others are also possible alternatives that preliminary results show improved H_2 uptake capacity.[22]

Yaghi and co-workers first carried out CO_2 uptake by MOF-177 in 2005 and a record capacity of 40 mmol g^{-1} or 390 cm^3(STP) cm^{-3} was obtained in NH_4F-treated MIL-101.[23] CH_4 storage has not been developed as rapidly as H_2 storage although its first measurement in a MOF was much earlier by Kitagawa and coworkers in 1997.[24] A Cu-based MOF, PCN-14, has been demonstrated to uptake an absolute CH_4 capacity of 230 v/v at 290 K and 35 bar, 28% higher than the DOE target (180 v/v) for methane storage, with the highest adsorption heat of CH_4 of ~30 kJ mol^{-1}, which holds the current record for CH_4 storage.[25]

2.1.2 Gas separation. The separation of CO_2 from CH_4 is an important process in natural gas upgrading because CO_2 reduces the energy content of natural gas and induces pipeline corrosion. Moreover, CO_2 is the predominant greenhouse gas causing global warming. Motivated by these considerations, the selective capture of CO_2 from gas mixtures (especially from CO_2/CH_4 and CO_2/N_2) have attracted the most attention among all gas separation studies over MOFs.[26] Very recently, Li and coworkers obtained the highest separation selectivity for CO_2 reported to date among all MOFs by using a flexible Zn-MOF with 1D micropore channels. They achieved a separation ratio of 294, 190, 257, and 441 (v/v) for CO_2/N_2, CO_2/H_2, CO_2/CH_4 and CO_2/CO, respectively, at 0.16 atm and 25 °C, whilst at 0.2 atm and 25 °C a 768 (v/v) for CO_2/O_2 was observed.[26f] There are also a couple of reports on selective separation for some other gases, such as, O_2, NO, *etc.*[27]

2.1.3 MOF membrane-based gas separation. It is worthy to note here that MOF membranes have emerged as a unique media for gas separation applications in the last two years.[28]

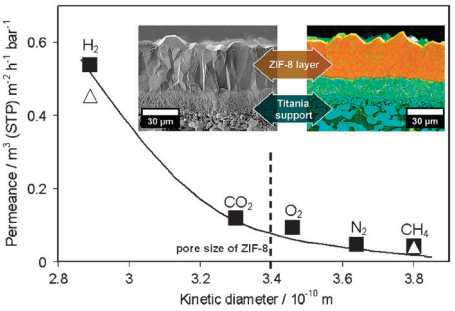

Fig. 2 Single (squares) and mixed (triangles) gas permeances for a ZIF-8 membrane *vs.* kinetic diameters. Inset: SEM image of the cross section of a simple broken ZIF-8 membrane (left) and EDS mapping of the sawn and polished ZIF-8 membrane (right, color code: orange, Zn; cyan, Ti). Adapted with permission from ref. 28*e*. Copyright 2009, American Chemical Society.

Liu *et al.* have synthesized the first continuous MOF-5 membranes by in situ solvothermal synthesis and measured the permeation of SF_6, CO_2, N_2, CH_4 and H_2, showing that these gases exhibit Knudsen diffusion behavior and size-selective permeability.[28a] Jeong and coworkers have obtained similar results for MOF-5 continuous membranes grown *via* microwave rapid seeding followed by solvothermal secondary growth.[28b] Guo *et al.* have presented the first MOF membrane to show gas-separation performance beyond Knudsen diffusion behavior. They used a copper net to provide homogeneous nucleation sites to support a continuous HKUST-1 film growth. The copper net supported HKUST-1 membrane exhibits a high permeation flux and excellent permeation selectivity for H_2 (H_2/N_2 selectivity: 7).[28c] Ranjan and Tsapatsis have prepared preferentially oriented and well-intergrown MOF films on porous α-alumina discs with ideal selectivity for H_2/N_2 as high as 23 *via* a seeded growth method.[28d] Caro and coworkers have systematically fabricated several ZIF (zeolitic imidazolate framework)-based membranes by previous seed coating or chemical modifications for the supports. The ZIF membranes exhibit high H_2 selectivities over other gases (Fig. 2).[28e–h] Venna and Carreon have synthesized ZIF-8 membranes with ~5–9 nm thickness by secondary seeded growth on tubular α-Al_2O_3 porous supports and confirmed their performances on CO_2/CH_4 separation.[28i]

In addition, the storage and separation for other gas molecules, such as, propane, propene, butane, *etc.*, have also been investigated.[29] There have been several reviews covering gas sorption and separation recently,[10c–e,15d,e] Hence, we herein do not discuss them in detail.

2.2 Chromatographic separation

The tailorable pores in MOFs make them great potential not only for small gas molecules storage and separation, but also for adsorption and separation of larger molecules, which also have interest although the reports are less than the former study.[9b,30] Chromatorgaphy (including gas- and liquid-phase) has become one of the most powerful tools in analytical chemistry. Usually, porous silica gel or alumina with modest surface areas (200–800 m^2 g^{-1}) and 5–25 nm of pore sizes are used as solid adsorbents.[31] The gel permeation

Downloaded by University of Science and Technology of China on 07/05/2013 04:06:21.
Published on 02 February 2011 on http://pubs.rsc.org | doi:10.1039/C0CC05419D

chromatography (GPC), generally with cross-linked styrenes as supports, are amorphous and have broad pore sizes, which are not preferable for highly selective separation of small molecules. Zeolites have defined nanostructures in a small pore regime. Unfortunately, they suffer from poor transport kinetics owing to restricted pore apertures and also cannot accommodate larger molecules for pharmaceutical and fine chemical uses. By contrast, porous MOFs could be good alternatives as stationary phases for chromatography, because they are crystalline and have high pore volume as well as tunable pore sizes/shapes.

To our knowledge, Chen *et al.* first employed MOF-508 (Zn(1,4-benzenedicarboxylate)(4,4′-bipy)$_{0.5}$), an interpenetrated MOF with 1D channels of approximately 4.0 × 4.0 Å in cross section, for gas chromatography (GC) separation of natural gas mixtures and alkane mixtures in 2006 (Fig. 3).[32] The authors have proposed that the selective GC separation of alkanes with a MOF-508 column is on the basis of their different van der Waals interactions with the microporous MOF-508 walls, which arise from the subtle matching of the size and shape of the alkanes with the MOF-508 micropores. Nuzhdin *et al.* presented the first example of a chiral chromatographic column for the separation of racemic mixtures of chiral alkyl aryl sulfoxides over an enantiopure porous MOF stationary phase in 2007, in which the homochiral 3D Zn-based MOF contains 1D chiral chains made up of chiral lactate and benzendicarboxylate ligands.[33] Enantiomeric excesses were the highest observed for those sulfoxides that had the most appropriate size and hence best fit the inner pores of the Zn-based MOF. This emphasized the key interplay of guest and pore shape in obtaining optimal results.[33b]

A 3D porous Zn-MOF is constructed from paddle-wheel $Zn_2(COO)_4$ clusters bridged by benzenedicarboxylate dianions and 1,4-diazabicyclo[2.2.2]octane as pillar linkers, which involves two types of intersecting channels of 7.5 Å × 7.5 Å along the *a*-axis and channels of 3.8 Å × 4.7 Å along the *b* and *c* axes, respectively.[34a] The authors have employed the Zn-MOF for the separation of hexane isomers *n*-hexane (*n*HEX), 3-methylpentane (3MP), and 2,2-dimethylbutane (22DMB). The different breakthrough times in the order *n*HEX > 3MP > 22DMB indicate that the adsorption strengths of the hexane isomers to Zn-MOF decrease as the degree of branching increases simply because of their different van der Waals interactions with the microporous walls and the confinement of *n*HEX within the small pores. *n*HEX can have the access to all three intersecting channels, thus its interaction with Zn-MOF is significantly stronger than the other two isomers.[34b] The application of a porous Co-MOF (CUK-1) as a gas chromatographic column filler has also successfully separated the light gases (H_2, O_2, N_2, CH_4 and CO_2).[35]

De Vos and coworkers have devoted much to this topic and achieved lots of interesting results.[36] They have firstly demonstrated the successful use of MIL-47 as a selective adsorbent for the extremely difficult and industrially relevant separations of *para*-xylene (*p*-xylene) *versus* *meta*-xylene (*m*-xylene) and *para*-xylene *versus* ethylbenzene. From breakthrough experiment profiles, the average selectivities were 2.5 : 1 for the separation of *p*-xylene and *m*-xylene, and 7.6 : 1 for the separation of *p*-xylene and ethylbenzene. In pulse chromatographic experiments with MIL-47, three well-separated peaks were obtained for the ternary mixture of ethylbenzene, *m*-xylene and *p*-xylene (Fig. 4). The selectivity for the mixture was due to a molecular packing effect inside the sterically confining environment of the pores in MIL-47. Rietveld refinement of powder X-ray diffraction patterns indicated that the selectivities were not due to interactions with the framework, but rather due to better packing of some isomers over others in the pores in MIL-47.[36a] They have also demonstrated that an optimal pore evacuation process for MIL-47 to remove the uncoordinated terephthalic acid at 300 °C highly affects the adsorption capacity and selectivity. Optimally activated MIL-47 is capable of selectively adsorbing the *p*-isomer from *p*-*m* mixtures of disubstituted aromatics like ethyltoluenes, xylenes, dichlorobenzenes, toluidines and cresols.[36b]

The porous MIL-53(Al) framework was investigated for selective adsorption and separation of xylenes and ethylbenzene (C8), ethyltoluenes (C9), and cymenes (C10) with batch, pulse chromatographic, and breakthrough experiments, and the results were compared with MIL-47.[36c] It has been found that MIL-53 has a particular preference for the adsorption of the *ortho*-isomer and it can separate the *ortho*-compounds from the other isomers whereas it was unable to discriminate between the *p*- and *m*-isomers. Rietveld refinement studies show that the geometry of *ortho*-xylene (*o*-xylene) allows for interaction between both methyl groups with the carboxylate groups in the structure, interactions which are not prevalent for the other isomers, revealing the

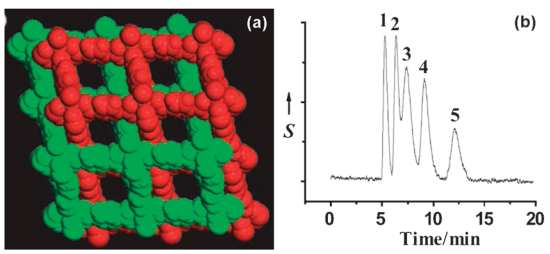

Fig. 3 (a) Space-filling representations of the structures of the open phase of MOF-508 with a 1D channel. (b) Chromatogram separated on a MOF-508 column for alkane mixtures: (1) 2-methylbutane, (2) *n*-pentane, (3) 2,2-dimethylbutane, (4) 2-methylpentane, and (5) *n*-hexane. S = thermal conductivity detector response. Adapted with permission from ref. 32. Copyright 2006, Wiley-VCH Verlag GmbH & Co. KGaA.

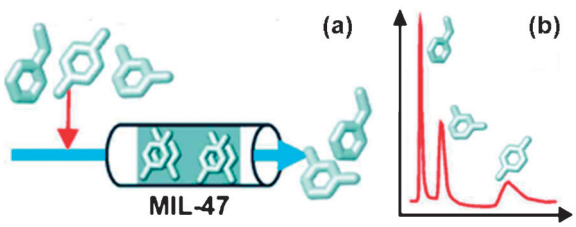

Fig. 4 (a) Schematic representation and (b) experimental results of a pulse chromatographic experiment using MIL-47 as sorbent for ethylbenzene, *m*-xylene, and *p*-xylene separation. Adapted with permission from ref. 36*a*. Copyright 2007, Wiley-VCH Verlag GmbH & Co. KGaA.

 This journal is © The Royal Society of Chemistry 2011

Downloaded by University of Science and Technology of China on 07/05/2013 04:06:21.
Published on 02 February 2011 on http://pubs.rsc.org | doi:10.1039/C0CC05419D

reason for the observed selectivities. When the same adsorption experiments as used with MIL-53 are conducted with MIL-47 as adsorbent, completely different adsorption preferences are obtained. MIL-47 preferred adsorption of *p*- and *m*-xylene over ethylbenzene and *o*-xylene and efficiently separated *p*- and *m*-xylene. Hence, MIL-53 and MIL-47 display very different selectivities and interaction mechanisms although they have very similar pore topography. It is proposed that the presence of different metals in the two materials might lead to a different polarization of the carboxylate groups. This results in the different separation mechanisms for the two adsorbents: efficient packing of the isomers within the pores leads to the observed selectivities in MIL-47 whereas interaction between the carboxylate groups of the framework and the adsorbates leads to the selectivity of MIL-53.[36c] Three porous MOFs with similar pore window diameters, HKUST-1, MIL-47 and MIL-53(Al), were compared for selective adsorption of olefins, alkylnaphthalenes and dichlorobenzenes in the liquid phase. Selective adsorption of olefins, preference for *cis*-olefins over *trans*-olefins, is observed on HKUST-1 due to the π-complexation on its open metal sites. All three MOFs have high affinities for alkylnaphthalene and dichlorobenzene isomers. For alkylnaphthalene and dichlorobenzene isomers, the identical preference orders found for all three materials whereas different underlying mechanisms were discussed.[36d] Both MIL-47 and MIL-53(Al) were found to be capable of separating ethylbenzene and styrene with different adsorption mechanisms. For MIL-47, diffraction experiments reveal that styrene is packed inside the pores in a unique, pairwise fashion, resulting in separation factors as high as 4 in favor of styrene. For MIL-53, the origin of the preferential adsorption of styrene is related to differences in enthalpy of adsorption, which are based on different degrees of framework relaxation. In addition, MIL-53 can also effectively remove typical impurities like *o*-xylene or toluene from styrene-ethylbenzene mixtures.[36e] Microporous MIL-96 as well as two zeolites with CHA and LTA topologies has been applied to a complex liquid-phase separation of isoprene, *cis*-piperylene and *trans*-piperylene. The investigation for adsorption selectivities on the various materials show that MIL-96 and chabazite preferentially adsorb *trans*-piperylene from a mixture containing all three C5-diolefin isomers with high separation factors and a higher capacity compared to the reference zeolite 5A due to a more efficient packing of the *trans* isomer in the pores. Moreover, MIL-96 is the only material capable of separating all three diolefin isomers from C5-mono-olefins and paraffins.[36f] Most recently, a silica-HKUST-1 composite was prepared *via* an impregnation method. The composite when used as a HPLC stationary phase combines the good column packing properties of silica and separation ability of HKUST-1, and thus shows the synergistic effects for the separation of ethylbenzene and styrene.[36g]

Denayer and coworkers have studied vapor-phase adsorption and separation of the C8 alkylaromatic components *p*-, *m*-, *o*-xylene, and ethylbenzene on MIL-47 and MIL-53.[37] The MIL-47 have successfully separated the different isomers. Results showed that the adsorption selectivity increased with degree of pore filling and is strongly dependent on pressure and temperature.[37a] For MIL-53, its separation mechanism is closely related to the state of the pore structure and pronounced framework breathing is observed during the adsorption of these substrates. With low pressure, adsorption brings in the framework contraction. In the closed form of the MIL-53 framework, it shows no difference for the isomers. Under higher pressure, the pores are induced to present the pen form of the MIL-53 framework. The space is large enough to adsorb xylene isomers in pairs along the length of the pores, resulting in a doubling of the amount adsorbed. Owing to the differences in the efficiencies with which the different isomers can be packed inside this larger space, differences in isotherm steepness and adsorption capacity arise. Such breathing phenomenon strongly influences the separation of molecular mixtures. With lower pressures than the transition pressure, no separation can be achieved. With higher pressures than the transition pressure, the adsorption selectivity increases along with the degree of pore filling.[37b] The combined experimental and simulation methods to investigate the low-coverage adsorption of MIL-47 for linear and branched alkanes have shown that the carbon number dependency of the low-coverage adsorption properties (Henry constants and adsorption enthalpy) match very well between the results from both methods.[37c]

Recently, Yan and coworkers became the first to fabricate a MOF-coated capillary column for high-resolution GC separation.[38] By choosing MIL-101[5a] as the stationary phase, a baseline separation of *p*-, *m*-, *o*-xylene, and ethylbenzene was achieved within 1.6 min without the need for temperature programming due to the difference in the polarity of these isomers. The MIL-101 coated capillary column was further demonstrated by high-resolution GC separation of two other isomer mixtures of substituted benzene derivatives, as well as a mixture of *n*-alkanes with a broad range of boiling points.[38a] A zeolite-type ZIF-8 nanocrystal coated capillary was fabricated, which exhibited a strong ability to sieve branched alkanes from linear alkane isomers due to the narrow pore windows, and also offered excellent features for high-resolution gas chromatographic separation of linear alkanes owing to van der Waals interaction between linear alkanes and the hydrophobic inner surfaces of the micropores.[38b] Matzger and coworkers have examined a series of porous MOFs as efficient adsorbents for removal of organosulfur compounds dibenzothiophene (DBT) and 4,6-dimethyldibenzothiophene (DMDBT) from model diesel fuel and diesel fuel (Fig. 5).[39a,b]

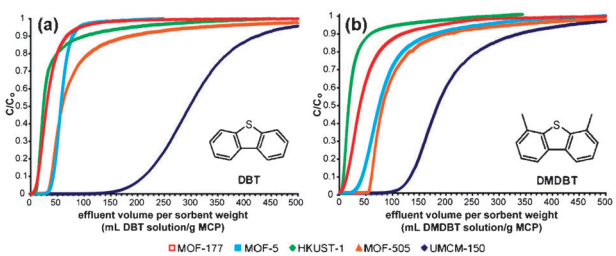

Fig. 5 Breakthrough curves for (a) 300 ppmw S DBT in isooctane and (b) 300 ppmw S DMDBT in isooctane for MOF-177, MOF-5, HKUST-1, MOF-505 and UMCM-150. Adapted with permission from ref. 39*b*. Copyright 2009, American Chemical Society.

Downloaded by University of Science and Technology of China on 07/05/2013 04:06:21.
Published on 02 February 2011 on http://pubs.rsc.org | doi:10.1039/C0CC05419D

The examined MOFs exhibit a good selectivity for the organosulfur compounds that is not seen in other materials, such as zeolites and activated carbon, which are also used for desulfurization. In addition, regeneration of porous MOFs packed beds has been shown to be feasible.[39b] The potential of HKUST-1 and MOF-5 as stationary phases in liquid chromatographic separations for some organic compounds has also been evaluated. For the separation of a mixture of benzene, naphthalene and anthracene, the larger the aromatic compound, the longer the retention time due to greater interactions with the HKUST-1 framework. While for a mixture of benzene, naphthalene and 1,3,5-triphenylbenzene, the latter was almost unretained due to the size exclusion effect. In addition, separation of ethylbenzene and styrene was very efficiently achieved using HKUST-1 due to interaction of π-complexation between styrene and the copper of the framework. The experimental results demonstrate the ability of porous MOFs to not only act as shape- and size-selective sorbents but also separate even molecules with very similar sizes if coordination differences can be exploited.[39c]

We have prepared three pillar-layered Cd(II)-MOF isomers from the same reaction starting materials but using slightly changed reaction conditions in each case. Interestingly, the three Cd-MOF isomers based on the same Cd_2 SBU and organic linkers are nonporous, microporous and mesoporous, respectively. The microporous Cd-MOF has 0.8×1.5 nm^2 free channels whereas the mesoporous one has larger 1D 1.7×2 nm^2 free channels (Fig. 6a and b). The two targeted dye molecules, rhodamine 6G (1.3×1.6 nm^2) and brilliant blue R-250 (1.8×2.2 nm^2), were successfully found to be effective for size-exclusion dominant liquid chromatographic (LC) separation by using the mesoporous Cd-MOF as a stationary phase whereas the microporous MOF with smaller pores does not work (Fig. 6c).[3g] As far as we know, this is the first report of a mesoporous MOF as an LC stationary phase for large dye

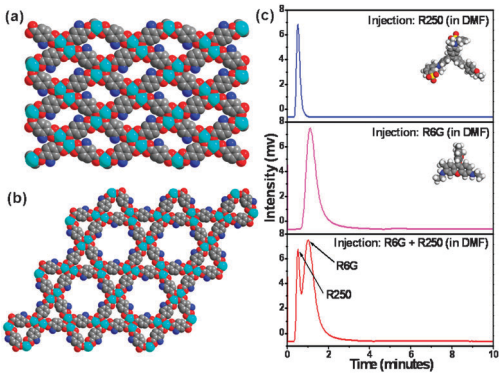

Fig. 6 Space-filling figures of the structures of (a) microporous and (b) mesoporous Cd-MOF isomers with different sizes of 1D channels along the *c*-aixs. (c) Chromatographic separation of brilliant blue 250 and rhodamine 6G achieved using mesoporous Cd-MOF as the stationary phase (the flow rate of mobile phase (DMF): 0.5 mL min^{-1}; detected wavelength: 540 nm). Adapted with permission from ref. 3*g*. Copyright 2010, American Chemical Society.

separation. Recently, Han *et al*. demonstrated that the chromatographic separations can be performed in single MOF crystals. They used millimeter-sized MOF-5 crystals as "columns" to separate mixtures of two or three organic dyes over distances of only a few hundred micrometers. Using fluorescent dyes in conjunction with fluorescence confocal microscopy, they have quantified the concentration profiles within the crystal and demonstrated that the efficiency of the separation derives from an interplay between the diffusive and capillary transport in addition to the fleeting noncovalent interactions between the migrating molecules and the MOF scaffold.[40]

The reported separations of various absorbate mixtures based on different porous MOFs as adsorbents have been summarized in Table 1. Although the chromatographic separations by porous MOFs started late in contrast to

Table 1 Separations of various absorbate mixtures studied by different MOFs as adsorbents.

MOF	Absorbent	Ref.
MOF-508	2-methylbutane, *n*-pentane, 2,2-dimethylbutane, 2-methylpentane, *n*-hexane	32
Zn-MOF	racemic mixture of chiral alkyl aryl sulfoxides	33*b*
Zn-MOF	*n*-hexane, 3-methylpentane, 2,2-dimethylbutane	34*b*
CUK-1	H_2, O_2, N_2, CH_4, CO_2	35
MIL-47	*o*-, *m*-, *p*-xylene, ethylbenzene	36*a*
MIL-47	*p*-*m* mixture of ethyltoluenes, xylenes, dichlorobenzenes, toluidines, cresols	36*b*
MIL-53, MIL-47	xylenes, ethylbenzene, ethyltoluenes, cymenes	36*c*
HKUST-1, MIL-47, MIL-53(Al)	olefins, alkylnaphthalenes, dichlorobenzenes	36*d*
MIL-47, MIL-53(Al)	ethylbenzene, styrene	36*e*
MIL-96	C5-hydrocarbons (isoprene, *trans*- and *cis*-piperylene)	36*f*
SiO_2-HKUST-1	ethylbenzene, styrene	36*g*
MIL-47	*p*-, *m*-, *o*-xylene, ethylbenzene	37*a*
MIL-53(Al)	*p*-, *m*-, *o*-xylene, ethylbenzene	37*b*
MIL-47	linear and branched alkanes	37*c*
MIL-101	*p*-, *m*-, *o*-xylene, ethylbenzene, *p*-, *m*-, *o*-chlorotoluene, 1,3,5-trimethylbenzene, *n*-propylbenzene, isopropylbenzene, *n*-alkanes	38*a*
ZIF-8	linear and branched alkanes	38*b*
MOF-177, MOF-5, HKUST-1, MOF-505, UMCM-150	dibenzothiophene and 4,6-dimethyldibenzothiophene in diesel fuel	39*b*
HKUST-1, MOF-5	benzene, ethylbenzene, styrene, naphthalene, phenanthrene, pyrene, 1,3,5-triphenylbenzene, anthracene, 1,3,5-tris(4-bromophenyl)benzene	39*c*
Cd-MOF	rhodamine 6G, brilliant blue R-250	3*g*
MOF-5	pyronin Y, pyronin B, thionin, toluidine blue O, azure A, brilliant green, and methyl yellow	40

 This journal is © The Royal Society of Chemistry 2011

Downloaded by University of Science and Technology of China on 07/05/2013 04:06:21.
Published on 02 February 2011 on http://pubs.rsc.org | doi:10.1039/C0CC05419D

their gas storage/separation behaviors, it opens a gateway to separation/purification sciences with a promising future. In many cases, porous MOFs have outperformed benchmark materials such as zeolites and activated carbons. Porous MOFs hold the advantages of alterable metal centers (or SBUs) and organic linkers as well as modifiable pore surface/space, which offer paths towards rationally tailoring not only pore sizes, structures and shapes but also interfacial properties. However, some porous MOFs are thermally and chemically unstable and sometimes scalable synthesis is problematic. To realize final industrial separation applications, besides the performance improvement, the stability and large-scale production of MOFs as well as their cost should be taken into account and further efforts made.

3. Heterogeneous catalysis

Heterogeneous catalysis is one of the most important, earliest proposed (20 years before) and developed applications (15 years before) of MOFs.[1b,9a] The wide range of adjustable metal centers and their surrounding environments as well as functionizable crystalline frameworks provide multiple opportunities to create desirable active sites for catalysis. Although zeolites have been regarded as one of the most commercially important catalysts, the small pore size of zeolites is usually a key limitation to address the catalytic reactions with large substrates, such as, polyaromatics, carbohydrates, and glycerides, *etc.*; while mesoporous silicate materials, such as the MCM- and SBA-series of materials, have pores that are too large which don't have confinement effects for catalytic substrates. Porous MOFs have an abundant diversity of structures and have extensively reported pore sizes ranging from non-pores to mesopores. Therefore, pore-size tunable MOFs are regarded as bridging the gap between zeolites and mesoporous silica[9c] and are very suitable in various catalytic reactions, including liquid- and gas-phase catalysis.

3.1 Liquid-phase catalysis

Liquid-phase catalysis has been very familiar in MOF-based catalysis since the first report of cyanosilylation of aldehydes by a layered MOF with the formula $Cd(4,4'\text{-bipyridine})_2(NO_3)_2$.[9a] A considerable amount of liquid-phase catalytic reactions over MOFs have been reported, mainly, Lewis acid-based carbonyl cyanosilylation and Mukiyama aldol reactions;[41] base-based Knoevenagel condensation;[42] hydrogenation;[43] hydrodesulfurization;[44] oxidation or epoxidative of olefins, sulfides and alkanes;[45] photocatalysis;[46] Friedel–Crafts benzylation and regioselective ring opening of epoxides over Fe-based MOFs,[47] *etc*. Since this topic has been systematically reviewed by several groups recently,[9c–f] we will not give more details here.

3.2 Gas-phase catalysis

In contrast to liquid-phase catalysis, gas-phase catalytic studies are very rare. Naito *et al*. have reported the first example of the preparation of 3D microporous MOFs, Rh-based fumarate and terephthalate complexes, which catalyzed the hydrogenation of gas-phase ethene, propene and butane molecules in 2001.[48] After evacuation, the Rh(II) fumarates and terephthalates exhibited high catalytic activity for H_2–D_2 exchange reactions even at 27 °C. Moreover, hydrogen exchange of olefins such as ethene, propene and butene as well as their hydrogenation took place at 27 °C while catalytic activity decreased gradually with repeated runs, possibly due to the accumulation of hydrocarbon byproducts. Experimental results indicate that the active sites for the hydrogen exchange of olefins exist only inside the micropores of the MOFs, while hydrogenation of olefins takes place both inside and at the outer surface of the MOFs. The dependence of the initial rates of hydrogenation and hydrogen exchange upon the sizes of the olefins and organic ligands was investigated by changing propene with ethene and butene, and also fumaric acid with terephathalic acid ligand. Smaller olefins and MOFs with larger ligands exhibited higher activities for hydrogen exchange and also larger olefin/Rh ratios, indicating that these reactions take place mainly inside the micropores of the MOFs.

Subsequently, Mori and co-workers prepared a series of microporous Rh-MOFs, Rh_2[MTCPP] (M = H_2, Cu^{2+}, Ni^{2+}, Pd^{2+}), based on H_2TCPP ligand (H_2TCPP = 4,4′,4″,4‴-(21*H*,23*H*-porphine-5,10,15,20-tetrayl)tetrakis benzoic acid). The MOFs having uniform micropores of *ca*. 5.0 Å show high surface areas and act as efficient heterogeneous catalysts for the hydrogenation of olefins at approximately −73 °C.[49] Hydrogenation of propene has been conducted at −79 °C, −53 °C and −18 °C, respectively and propane with 100% selectivity at all reaction temperatures was obtained as the product. At −79 °C, the order of the activity of these MOFs for propene hydrogenation was $Pd^{2+} > Cu^{2+} > Ni^{2+} \gg H_2$. The catalytic results at −53 °C and -18 °C also showed that the Pd-containing MOF was the most active and the order of the activity was the same ($Pd^{2+} > Cu^{2+} > Ni^{2+} > H_2$). As displayed in Fig. 7, these bimetallic effects of Cu–Rh, Ni–Rh, and Pd–Rh were not dependent on the BET surface area, but rather dependent on the type of metal atoms centered in the porphyrin ring. In addition, all these MOFs were also observed to catalyze the hydrogenation of 1-butene to butane (100% selectivity) at −53 °C and −18 °C and the order of the activity at both temperatures similarly was $Pd^{2+} > Cu^{2+} \geq Ni^{2+} > H_2$. Moreover, no nonporous rhodium carboxylate

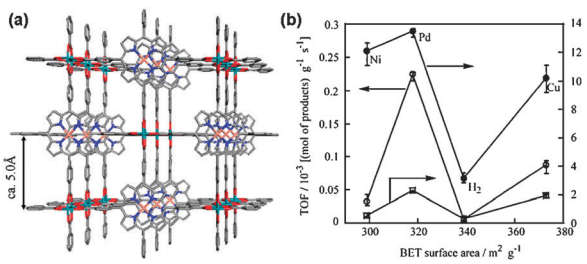

Fig. 7 (a) Deduced molecular structure of Rh_2[MTCPP] (M = H_2, Cu^{2+}, Ni^{2+}, Pd^{2+}). Elements are color-coded: Rh (green), C (gray), N (blue), O (red), and M (pink). (b) Surface area dependence of turnover frequency (TOF) for propene hydrogenation catalyzed by Rh_2[MTCPP] (M = H_2, Cu^{2+}, Ni^{2+}, Pd^{2+}) at −79 °C (○), −53 °C (□), and −18 °C (●). Adapted with permission from ref. 49*b*. Copyright 2005, Elsevier.

Downloaded by University of Science and Technology of China on 07/05/2013 04:06:21.
Published on 02 February 2011 on http://pubs.rsc.org | doi:10.1039/C0CC05419D

MOF showed any reaction for the hydrogenation of propene at −79 °C. Based on the obtained results, it is concluded that (a) the hydrogenation reactions requires Rh centers, (b) the intramolecular distances between the metal atoms centered in the porphyrin ring and the Rh centers are critical for the hydrogenation reactions, and (c) the hydrogenation reaction occurs in the micropores.[49b]

Our group has firstly applied porous MOFs as active catalysts for CO oxidation.[50] The reaction is useful for its implications in the production of clean hydrogen for the chemical industry from hydrocarbon feeds and has been intensively investigated by metal catalysts, especially for Au NPs-supported metal oxide catalysts.[51] Solvothermal reactions of $Ni(NO_3)_2$, 4,5-imidazoledicarboxylic acid (H_3L), and LiOH or NaOH in H_2O/CH_3OH at 90 °C afforded two crystalline porous MOFs: $\{[Li_{11}(Ni_8L_{12})(H_2O)_{12}]Li_9(H_2O)_{20}\}_n$ and $\{[Na_{20}(Ni_8L_{12})(H_2O)_{28}](H_2O)_{13}(CH_3OH)_2\}_n$, respectively with considerable surface areas. Both structures consist of $[Ni_8L_{12}]^{20-}$ cubic building blocks bridged by Li^I or Na^I ions. The Na-containing MOF exhibits stable catalytic activity in the oxidation of CO to CO_2 whereas the Li-containing MOF lacks such activity probably due to its lower thermal stability. The Na-containing MOF showed stable activity for the initial 20 min of reaction time at a fixed temperature of 202 °C or higher. The PXRD patterns indicate that the MOF framework remains intact after the catalytic reaction and that no crystalline NiO is present.[50a]

The metal centers in MOFs are usually coordinated with not only organic linkers but also solvents (such as, water, DMF, *etc.*). The frameworks of thermally robust MOFs can remain stable upon solvent removal, leaving the exposed metal centers. The exposed metal centers inside channels or cavities of porous MOFs are freely accessible to catalytic substrates as catalytic active Lewis acid sites. With this strategy, our group have prepared $[Cu(mipt)(H_2O)](H_2O)_2$ (mipt = 5-methyl-isophthalate), the framework of which exhibits two types of 1D channel and contains paddle-wheel Cu_2 clusters interconnected by bent mipt linkers to form an undulating 2D net with 4^4 topology (Fig. 8a).[50b] Each Cu(II) center has a square-pyramidal coordination environment with coordinated H_2O as the pyramid and the two copper atoms share four carboxyl mipt ligands. The Lewis acid coordination sites are on the interior of the channel walls, and thus, the copper sites are accessible for adsorption and catalytic conversions. The accessibility of the copper sites after water elimination was demonstrated by FTIR spectroscopy using CO as a probe molecule at room temperature. A ν(C–O) stretching band was observed at 2113 cm^{-1} after ^{12}CO adsorption, which was assigned to CO adsorbed onto Cu Lewis acid sites. This band shifted to 2064 cm^{-1} when ^{13}CO was used (Fig. 8b). Fig. 8c shows the arrhenius plot of CO oxidation over the desolvated MOF compared with CuO, CuO/Al_2O_3, nanoCuO as well as the Ni-containing MOP reviewed above. The current MOF presents higher activity and its CO conversion reaches 100% at 200 °C, much higher than the Ni-containing MOP (3%).[50a] Moreover, the activity is similar or higher than that of CuO or CuO/Al_2O_3, and the activation energy (70.1 kJ mol^{-1}) is close to CuO (69.9 kJ mol^{-1}). Although room-temperature oxidation of CO is reported over CuO, the catalytic feature greatly

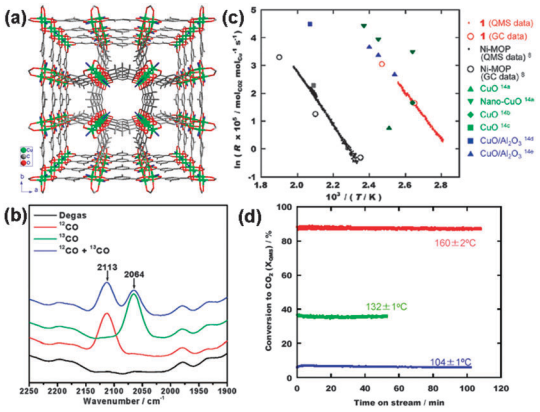

Fig. 8 (a) View of the MOF framework along the *c*-axis showing the paddle-wheel Cu_2 clusters and open channels. The oxygen of coordinated H_2O is highlighted as blue. The hydrogen atoms and isolated H_2O are omitted for clarity. (b) FTIR spectra of CO adsorbed on the MOF framework at room temperature (2113 cm^{-1} for ^{12}CO and 2064 cm^{-1} for ^{13}CO). (c) Arrhenius plots of CO oxidation over correlated catalysts (**1** presents the Cu-MOF). (d) Catalytic activity in CO oxidation at 104, 132, and 160 °C, measured on a flowing CO (1%) + O (20%) + He (balance) gas mixture (SV = 20 000 mL h^{-1} g(cat.)$^{-1}$). Adapted with permission from ref. 50*b*. Copyright 2007, American Chemical Society.

decreases upon exposing the sample to atmospheric air for a very short time (10–15 s). The nanoCuO showed much higher activity at 105 °C than the present MOF, while their activities are almost similar above 130 °C, which may be ascribed to the aggregation of nanoCuO samples at higher temperatures. In addition, it is worthy to note that the activity over the MOF is stable with time at a fixed temperature of 104 °C or higher (Fig. 8d). The sample also presents high stability when exposed to atmospheric air. The framework remains intact after catalytic reaction, demonstrating that the paddle-wheel Cu_2 clusters present the stable active sites for CO catalytic oxidation.

Currently, MOFs have been used as active and selective catalysts for a wide variety of reactions, from liquid to gas phases. However, the reported catalytic studies on MOFs are mostly limited to some very direct applications and more remain to be exploited. Although inferior to zeolites in thermal or chemical stability, porous MOFs present tunability, homochirality, highly regular catalytic sites, and original flexibility, which make them unique advantageous for the design of desirable MOF-based catalysts and allow the assessment of structure–activity relationships. One can definitely anticipate that porous MOFs have a bright future in heterogeneous catalysis.

4. Porous MOFs as supports/host matrices for metal NPs

In the last two decades, metal NPs supported on or incorporated into metal oxides, zeolites, mesoporous silica, and activated carbons have been widely studied as catalysts. Porous MOFs are thermally robust and have permanent nanoscale cavities or open channels, analogous to zeolites. Therefore, porous MOFs offer congenital conditions for embedding small NPs, and it is expected that the crystalline porous structures of MOFs limit the migration and aggregation of small metal

 This journal is © The Royal Society of Chemistry 2011

clusters/NPs, making MOF highly potential as support/host matrix for metal NPs.

4.1 Preparation methods

It has been reported that solution-, gas- and solid-phase loading methods all work well for the successful preparation, dependent on the different metal precursors (Table 2).

4.1.1 Solution method—Incipient wetness impregnation and coprecipitation and colloid deposition. The incipient wetness impregnation method is a mostly accepted method to prepare metal NPs deposited to MOFs, in which common inorganic salts are adoptable as precursors. Suh and coworkers have obtained a series of porous MOF-based nanocomposites containing small Au or Ag or Pd NPs based on a redox

Table 2 Reported metal NPs/MOFs *via* various methods and for different applications

Preparation method	Metal precursor	Sample	Reduction method	Metal particle size (nm)	Application	Ref.
Incipient wetness impregnation	$AgNO_3$	Ag/[{Ni($C_{10}H_{26}N_6$)}$_3$(bpdc)$_3$]	autoredox	3	—	52*a*
	$AgNO_3$	Ag/[{Ni(cyclam)}$_2$(bptc)]	autoredox	4	—	52*b*
	$NaAuCl_4{\cdot}2H_2O$	Au/[{Ni(cyclam)}$_2$(bptc)]	autoredox	3.7 ± 0.4	—	52*b*
	$Pd(NO_3)_2{\cdot}2H_2O$	Pd/[{Ni(cyclam)}$_2$(mtb)]	autoredox	2.0 ± 0.6	—	52*c*
	$Pd(NO_3)_2{\cdot}2H_2O$	Pd@[SNU-3]$^{0.54+}$(NO_3^-)$_{0.54}$	autoredox	3.0 ± 0.4	Hydrogen storage	20*c*
	$Pd(NO_3)_2{\cdot}2H_2O$	Pd/{[Ni($C_{20}H_{32}N_8$)]$_2$[TCM]}	autoredox	2.9 ± 0.4	—	52*d*
	$AgNO_3$	Ag@MOF-508 Ag@MIL-68(In) Ag@HKUST-1	in the presence of EtOH	20 (TEM); 1–2 (EPR)	—	53
	$Pd(acac)_2$	Pd@MOF-5	H_2, 150 or 200 °C	—	Hydrogen storage; Catalytic hydrogenation	20*a*,54
	$Pd(acac)_2$	Pd@MIL-101	H_2, 200 °C	—	Catalytic hydrogenation of styrene	54
	$PdCl_2$, H_2PtCl_6	Pd@MIL-101	$NaBH_4$	2–4	Catalytic Knoevenagel condensation and Heck reactions	55*a*
	$Pd(NO_3)_2{\cdot}2H_2O$	Pd/MIL-101	$N_2H_4{\cdot}H_2O$, microwave	2–6	Catalytic CO oxidation	55*b*
	$Pd(NO_3)_2{\cdot}2H_2O$, $Cu(NO_3)_2$	PdCu/MIL-101	$N_2H_4{\cdot}H_2O$, microwave	1–6	Catalytic CO oxidation	55*b*
	H_2PtCl_4	Pd/MIL-100(Al)	H_2, 280 °C	1.8 ± 0.4	Hydrogen storage	20*d*
	$Pd(NO_3)_2{\cdot}2H_2O$	Pd/MIL-101	H_2, 200 °C	1.9 ± 0.7	Catalytic Suzuki-Miyaura and Ullmann coupling reactions	55*c*
	$Pd(NO_3)_2{\cdot}2H_2O$	Pd@MIL-101	H_2, 200 °C	2.5 ± 0.5	Catalytic synthesis of methyl isobutyl ketone	55*d*
Co precipitation	$Pd(NO_3)_2{\cdot}2H_2O$	Pd@MOF-5	—	—	Catalytic ethyl cinnamate hydrogenation	56*a*
Colloid deposition	$HAuCl_4{\cdot}4H_2O$	Au/MIL-101	$NaBH_4$	2.35 ± 1.08	Catalytic aerobic alcohol oxidation	56*b*
Gas-phase loading	CpPd(η^3-C_3H_5)	Pd@MOF-5	H_2, −35 °C	1.4 ± 0.1	Catalytic cyclooctene hydrogenation	57*a*
	CpCu(PMe_3)	Cu/MOF-5	H_2, 150 °C	3–4	Catalytic MeOH synthesis	57*a*
	(CH_3)Au(PMe_3)	Au/MOF-5	H_2, 190 °C	5–20	Inactive in catalytic CO oxidation	57*a*
	CpPd(η^3-C_3H_5)	Pd@MOF-5/SAM	photolysis	—	—	57*b*
	CpPd(η^3-C_3H_5)	Pd@MOF-177	photolysis	~3	—	57*c*
	CuCp(CN*t*Bu)	Cu@MOF-177	H_2, 220 °C	2–3	—	57*c*
	Me_3PtCp'	Pt@MOF-177	H_2, 100 °C	2–3	Catalytic alcohol oxidation	20*b*
	Ru(cod)(cot)	Ru@MOF-5	H_2, 150 °C	1.5–1.7	Catalytic alcohol oxidation	57*d*
	CpPd(η^3-C_3H_5)	Pd@MOF-5	photolysis	2.4 ± 0.2	—	57*e*
	Ru(cod)(cot), Pt(cod)Me_2	RuPt@MOF-5	H_2, 150 °C	4–6	—	57*f*
	Ni(η^5-C_5H_5)$_2$	Ni@MesMOF-1	H_2, 95 °C	1.4–1.9 (calc.)	Catalytic reduction of styrene and nitrobenzene	57*g*
	(CO)AuCl	Au@ZIF-8	H_2, 100 °C	1–5	Catalytic alcohol oxidation	57*h*
	(CO)AuCl	Au@ZIF-90	H_2, 130 °C	1–2	Catalytic alcohol oxidation	57*h*
Solid grinding	(CH_3)$_2$Au(acac)	Au@CPL-1	H_2, 120 °C	—	Catalytic alcohol oxidation	58*a*
		Au@HKUST-1	H_2, 120 °C	—	Catalytic alcohol oxidation	58*a*
		Au@MOF-5	H_2, 120 °C	3.3 ± 2.3	Catalytic alcohol oxidation and *N*-alkylation of amine and alcohol	58*a*,58*b*
		Au@CPL-2	H_2, 120 °C	2.4 ± 1.0	Catalytic alcohol oxidation and *N*-alkylation of amine and alcohol	58*a*,58*b*
		Au@MIL-53(Al)	H_2, 120 °C	1.5 ± 0.7; 1.6 ± 1.0	Catalytic alcohol oxidation and *N*-alkylation of amine and alcohol	58*a*,58*b*
		Au@ZIF-8	H_2, 230 °C	~3	Catalytic CO oxidation	58*c*
		Au@Cd-MOF	H_2, 170 °C	ultrafine	—	58*d*

Published on 02 February 2011 on http://pubs.rsc.org | doi:10.1039/C0CC05419D
Downloaded by University of Science and Technology of China on 07/05/2013 04:06:21.

Downloaded by University of Science and Technology of China on 07/05/2013 04:06:21.
Published on 02 February 2011 on http://pubs.rsc.org | doi:10.1039/C0CC05419D

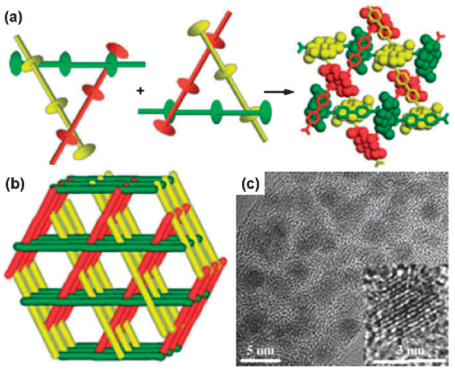

Fig. 9 (a) Double network of threefold braids of a Ni-MOF structure where macrocycles fit into the grooves created by $bpdc^{2-}$ ligands. (b) View showing the stacking of the linear chains to generate 1D channels. (c) HRTEM images of the solid isolated after immersion of the desolvated Ni-MOF in $AgNO_3$ (8.0×10^{-2} M) methanolic solution for 10 min at room temperature. Adapted with permission from ref. 52*a*. Copyright 2005, Wiley-VCH Verlag GmbH & Co. KGaA.

reaction of Ni(II)-MOF in the absence of additional reducing and capping agents.[52] They first prepared Ag NPs-MOF nanocomposites from a redox-active porous MOF, $[\{Ni(C_{10}H_{26}N_6)\}_3(bpdc)_3]\cdot 2C_5H_5N\cdot 6H_2O$ (bpdc = 4,4′-biphenyldicarboxylate).[52*a*] The Ni-MOF with 1D channels is constructed by packing of the linear coordination polymer chains formed from the nickel macrocyclic complex $[Ni(C_{10}H_{26}N_6)](ClO_4)_2$ and $bpdc^{2-}$ ions in a water/pyridine mixture (Fig. 9a and b). After desolvation, the Ni-MOF immersed in $AgNO_3$ methanolic solution at room temperature afforded the Ag NPs-MOF nanocomposite with Ag NP of sizes ~3 nm due to the redox reaction between Ag^+ ions and the Ni(II) macrocycles of the host. High-resolution TEM (HRTEM) images confirmed the production of Ag NPs (Fig. 9c). The PXRD patterns of the Ni-MOF remained after it was immersed in the Ag^+ solution for 10 min, indicating the retained structure. However, the PXRD patterns changed completely and became much weaker and broader after immersion for 18 h, suggesting that the destroyed host structure. The authors propose that the Ag^0 atoms initially collect in the channels, then diffuse into the surface of the host solid where they aggregate to form NPs under the stabilization of the $bpdc^{2-}$ ligands until the framework is destroyed. In addition, the authors have also successfully obtained the host-free Ag NPs with ~3 nm in diameter capped with long-chain carboxylic acids by treating the nanocomposite in boiling dioctyl ether (at ~290 °C) in the presence of oleic acid.

With a similar strategy, they prepared Ag (3.7 ± 0.4 nm) and Au (2 nm) NPs, respectively, by the redox reactions of $AgNO_3$ and $NaAuCl_4\cdot 2H_2O$ with a 2D square-grid MOF, $[Ni(cyclam)]_2(BPTC)\cdot 2H_2O$ (cyclam = 1,4,8,11-tetraazacyclotetradecane, H_4BPTC = 1,1′-biphenyl-2,2′,6,6′-tetracarboxylic acid) in 5 min.[52*b*] Different from the aforementioned case, the present MOF host framework remains even after immersed in Ag(I) solution for 16 h and Au(III) solution for 46 h, respectively, indicating that the host framework is stable to the redox reaction. Based on the detailed studies, the authors suggest that (a) both the open structure and the redox-active Ni(II) macrocyclic component are necessary for obtaining the monodispersed and small metal NPs; (b) the metal ions are introduced between the layers of the host framework to react with the Ni(II) species and then reduced to Ag(0) or Au(0) atoms, which diffuse to the surface of the host to aggregate as NPs. Following this research line, they subsequently fabricated Pd NPs-MOF composites with Pd NP sizes of around 2–3 nm with different Ni(II)-MOFs including macocyclic or N-containing redox-active ligands.[20*c*,52*c*,*d*]

Allendorf and coworkers reported a systematic investigation of Ag nanocluster formation within MOFs using three MOF templates, HKUST-1, MOF-508 and MIL-68(In).[53] The MOF templates were infiltrated in the aqueous-ethanolic solution of $AgNO_3$ and reduced to Ag NPs. Time-dependent TEM observations coupled with selected area electron diffraction (SAED) patterns show that the as-synthesized Ag clusters in the MOF are much smaller than the particles revealed by extended exposure to the beam. Initially, the Ag clusters are too small to be readily imaged with a defocused TEM beam, while the MOF crystal structure begins to break down almost immediately (within a few seconds to at most 1 min) upon illumination with the electron beam. After the crystal structure has broken down, the infiltrated Ag begins to coalesce until NPs of 2–5 nm are formed, at which point the resulting structure becomes stable in the electron beam. So the large particles observed by TEM are the result of damage to the MOF by the electron beam. The authors employed electron paramagnetic resonance (EPR) spectroscopy to confirm the presence of paramagnetic Ag_3^0 clusters throughout MOF-508 and MIL-68 templates. Electron tomography demonstrates that Ag NPs are thoroughly dispersed throughout the template and vibrational spectroscopy supports that the pore-included Ag clusters are small in size (Raman) and well distributed throughout the MOF (FTIR). FTIR analyses also demonstrate the ability of the MOF to chemically constrain the agglomeration of Ag.[53] Palladium was infiltrated into two typical porous MOFs, MOF-5 and MIL-101, by using $Pd(acac)_2$ (acac = acetylacetonate) as a precursor in chloroform solution *via* incipient wetness impregnation and followed by H_2 reduction.[20*a*,54] Chang and Férey *et al*. have realized metal encapsulation with a metal precursor-impregnation method by pre-grafting an amine on coordinatively unsaturated metal centers in a MOF. The pre-activated MIL-101 with numerous potential unsaturated chromium sites could be Lewis acid sites and usable for surface functionalization. After grafting ethylenediamine on unsaturated Cr(III) centers and the neutralization of the surface amine groups with an aqueous HCl solution, the positively charged surface ammonium groups undergo ionic reactions with anionic noble metal salts, such as, $PdCl_4^{2-}$, $PtCl_6^{2-}$, $AuCl_4^-$, by anionic exchange of the chloride anions, and are finally reduced by $NaBH_4$ at low temperature. The MIL-101 framework remains after the encapsulation of noble metals. TEM images for 1 wt% Pd@MIL-101 materials show that Pd NP sizes are in the range of 2–4 nm, in agreement with the cage diameters (2.9 and 3.4 nm), although some NPs still remain outside the pores. The formation of much larger Pd NPs (>20 nm) in MIL-101 without pre-grafting of amine further verifies the superior effect of amine-grafting to encapsulation of noble metals.[55*a*] Small Pd, Cu and Pd–Cu NPs of 2–3 nm

 This journal is © The Royal Society of Chemistry 2011

Downloaded by University of Science and Technology of China on 07/05/2013 04:06:21.
Published on 02 February 2011 on http://pubs.rsc.org | doi:10.1039/C0CC05419D

incorporated within the pores and larger particles of 4–6 nm supported on the surface of MIL-101 are obtained by immersing palladium or/and copper nitrates into an aqueous dispersion of MIL-101, followed by a reduction combining hydrazine hydrate and microwave radiation.[55b] The Pd@MIL-101 and Pd@MIL-100 nanocomposites with small Pd sizes have also been prepared by impregnation of activated MIL-101 or MIL-100 with palladium precursor solutions ($Pd(NO_3)_2$ or H_2PtCl_4), followed by hydrogen reduction.[20d,55c,d]

The other solution methods, such as, coprecipitation and colloidal deposition, have also been developed to obtain metal NPs/MOF nanocomposites.[56] The 0.5 wt% Pd NPs supported on MOF-5 were synthesized at 60 °C by a coprecipitation method, but without mention of the reduction method and Pd NP size distributions.[56a] Liu *et al.* prepared Au/MIL-101 by colloidal deposition with PVP as the protecting agent. The authors have found the method is the most efficient method to deposit fine Au NPs (2.35 ± 1.08 nm) onto MIL-101 and is superior to other methods they used, such as, impregnation or deposition-precipitation or colloidal deposition with glucose as the protecting agent.[56b]

4.1.2 Gas-phase loading method. Fischer and coworkers firstly worked on metal organic chemical vapor deposition (MOCVD) or gas-phase loading methods to prepare metal@MOF by using metal organic precursors and since 2005 they have developed a series of metal@MOF nanocomposites.[57a–f,h] The authors firstly employed MOF-5 as a host framework to support Pd, Au and Cu NPs. The activated MOF-5 was exposed to the vapor of the metal precursor ($CpPd(\eta^3\text{-}C_3H_5)$, ($CpCu(PMe_3)$ and (CH_3)$Au(PMe_3)$ for Pd, Au and Cu, respectively) in a static vacuum in a tightly sealed Schlenk-tube, and then the precursor was introduced into the pores of the MOF-5 in several minutes (Fig. 10). The metal@MOF formed after H_2 reduction. It is found that PXRD characteristic reflections of Pd@MOF-5 are significantly reduced or completely missing whereas high surface area (1600 $m^2\ g^{-1}$) is still found. In contrast, Cu@MOF-5 and Au@MOF-5 leave the crystalline host lattice completely intact.[57a] After depositing MOF-5 films on Al_2O_3 substrate, they loaded the same Pd precursor by MOCVD method and followed it by photolysis in an inert gas stream to yield the Pd-loaded thin film material Pd@MOF-5/Al_2O_3.[57b]

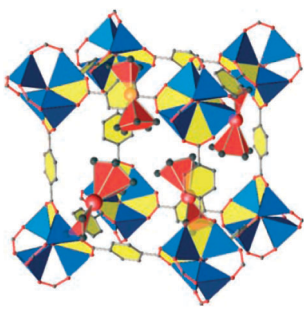

Fig. 10 MOF-5 cage (blue/yellow) with four incorporated $CpPd(\eta^3\text{-}C_3H_5)$ precursors (red). The elemental cell of the crystalline MOF-5 contains eight cavities of this kind. Reproduced with permission from ref. 57*a*. Copyright 2005, Wiley-VCH Verlag GmbH & Co. KGaA.

Highly porous MOF-177 has larger cavities and pore openings compared with MOF-5, which is possibly accessible for larger metal organic precursors and allows higher loadings of precursors. The CpCuL (L = PMe_3, CN*t*Bu) and $CpPd(\eta^3\text{-}C_3H_5)$ were loaded to desolvated MOF-177 *via* solvent-free adsorption from gas-phase. The analytical results show that the host lattice and the guest molecules interact only by weak van-der-Waals forces without any significant change to the framework or the chemical nature of the included molecules. After thermal hydrogenolysis at 220 °C and UV-light irradiation for Cu- and Pd-percursor loaded MOF-177, respectively, metal@MOF-177 materials were obtained. Detailed characterizations show that the Cu/Pd NPs are around 3 nm and the MOF-177 matrix remained unchanged during the NPs formation.[57c] With similar preparation methods mentioned above, the authors subsequently prepared more such materials with detailed characterizations. A typical size range of 1.5–1.7 nm of Ru NPs embedded in the intact MOF-5 framework were successfully obtained *via* gas-phase loading of MOF-5 with the volatile compound Ru(cod)(cot) (cod = 1,5-cyclooctadiene, cot = 1,3,5-cyclooctatriene) and followed by hydrogenolysis of the adsorbed Ru complex inside the pores.[57d] Four molecules of $CpPd(\eta^3\text{-}C_3H_5)$ were loaded into MOF-5 *via* gas-phase infiltration at 10^{-3} mbar and homogeneously distributed Pd NPs of 2.4 ± 0.2 nm can be achieved by photolysis of the inclusion compounds $[CpPd(\eta^3\text{-}C_3H_5)]_x$@MOF-5 ($x \leq 4$). The pure Pd_x@MOF-5 materials proved to be stable under hydrogen pressure (2 bar) at 150 °C over many hours. However, raising the Pd loading of a representative sample Pd_4@MOF-5 (35 wt% Pd) by using $CpPd(\eta^3\text{-}C_3H_5)$ as the precursor in a 2nd cycle of the gas-phase infiltration and photolysis led to the collapse of the long-range crystalline order of the MOF-5.[57e] Simultaneous gas-phase loading of Ru(cod)(cot) and $Pt(cod)Me_2$ into desolvated MOF-5 and subsequent hydrogenolysis resulted in the formation of alloyed PtRu NPs whereas the organic linkers of the MOF-5 were partially hydrogenated which caused a severe distortion of the MOF-5 matrix and loss of long range crystalline order.[57f] Very recently, they chose the chemically robust ZIF-8 ($Zn(MeIM)_2$, IM = imidazolate) and ZIF-90 ($Zn(ICA)_2$, ICA = imidazolate-2-carboxyaldehyde) as host matrices to capture Au NPs *via* gas phase infiltration of Au(CO)Cl precursor followed by a hydrogenation reduction. Low-dose HRTEM and electron tomography reveal a homogeneous distribution of Au NPs throughout the ZIF matrix. The functional groups of ZIF-90 direct the anchoring of intermediate Au species and stabilize smaller and quite monodisperse Au NPs in contrast to the non-functionalized ZIF-8.[57h]

In addition, Kempe and coworkers prepared Pt@MOF-177 with 2–5 nm Pt NPs embedded in the unchanged MOF-177 host framework *via* gas-phase loading of Me_3PtCp' (Cp′ = methylcyclopentadienyl) precursor and subsequent hydrogen reduction at 100 bar and 100 °C.[20b] Kim and coworkers have obtained Ni@MOF by introducing nickelocene into the evacuated MesoMOF-1 ($Tb_{16}(TATB)_{16}$, TATB = triazine-1,3,5-tribenzoate)[3e] *via* gas-phase loading and followed by

Downloaded by University of Science and Technology of China on 07/05/2013 04:06:21.
Published on 02 February 2011 on http://pubs.rsc.org | doi:10.1039/C0CC05419D

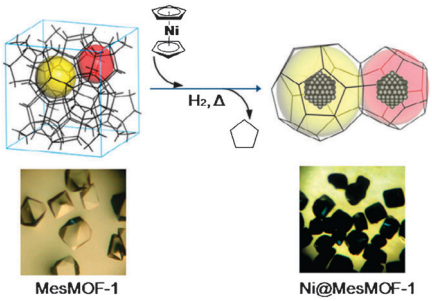

Fig. 11 A two-step procedure for the preparation of Ni@MesMOF-1 is schematically shown with pictures of the crystals before and after Ni embedment. Reproduced with permission from ref. 57*g*. Copyright 2010, The Royal Society of Chemistry.

hydrogen reduction (Fig. 11). The calculated sizes of Ni NPs ranged from 1.4 (Ni_{147}) to 1.9 nm (Ni_{309}).[57g]

4.1.3 Solid grinding method. In contrast to solution- and gas-phase methods, solid grinding is a very facile yet effective method for depositing metal NPs onto MOFs and was developed late in 2008. So far, only the volatile organogold complex, $Me_2Au(acac)$ (acac = acetylacetonate), has been studied as a Au precursor, which is easily reacted/absorbed on the surface of support.[58] Haruta and coworkers deposited Au clusters on several MOFs with 1D channels (MIL-53(Al); CPL-1: $Cu_2(pzdc)_2$(pyrazine); CPL-2: $Cu_2(pzdc)_2$(4,4′-bipyridine), pzdc = pyrazine-2,3-dicarboxylate)) or 3D channels (MOF-5, HKUST-1) by a solid grinding method followed by H_2 reduction. For comparison, supported Au catalysts were also prepared by CVD and by the deposition reduction from an aqueous solution containing $HAuCl_4$ and $NaBH_4$. They found Au/CPL-2 obtained *via* solid grinding gave Au NPs in nearly uniform cluster sizes of 2.2 ± 0.3 nm whereas CVD yielded larger Au NPs of 3.1 ± 1.9 nm. Moreover, the size of Au NPs strongly depends on the kinds of MOFs, metallic species, porous structures and pore sizes.[58a,b] Considering the longest dimension of a $Me_2Au(acac)$ molecule is ~6.5 Å, which is smaller than the pore opening (near to 8 Å) of ZIF-8 along the (111) direction, it thus can be absorbed into the cavities of ZIF-8. With this in mind, we prepared Au@ZIF-8 nanocomposites *via* a solid grinding method. The Au NP sizes showed a slight increase from 1 wt% (3.4 ± 1.4 nm) to 5 wt% (4.2 ± 2.6 nm) Au loadings.[58c]

More recently, we have prepared a 3D porous Cd-MOF ($Cd_2(L)(H_2O)\cdot 0.5H_2O$, L = 4,4′-(hexafluoroisopropylidene)-diphthalate) with two types of 1D channels, of which the larger one with a free diameter of 7.8 Å is fluorous and hydrophobic whereas the smaller one with an inner free dimension of 6.3 × 6.3 $Å^2$ is hydrophilic (Fig. 12a). The Cd-MOF has permanent porosity and presents an unprecedented hexagonal (4,8)-connected topology (Fig. 12b). Remarkably, by the facile solid grinding method, ultrafine Au_2 and Au_3 clusters incorporated into the porous structure has been demonstrated by TEM, HRTEM and XAFS (X-ray absorption fine structure) characterization (Fig. 12c and d). The Au clusters are fully unobservable by TEM and high-angle annular dark-field scanning transmission electron microscopy (HAADF-STEM) whereas energy dispersive spectroscopy

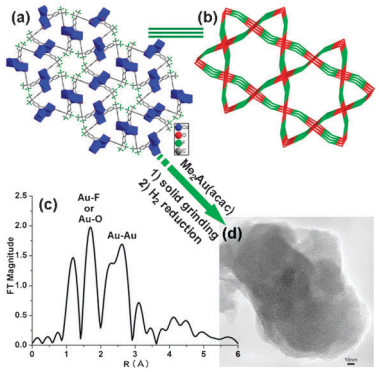

Fig. 12 (a, b) View and topological view of the 3D network of Cd-MOF along the *c*-axis. The H atoms and isolated H_2O are omitted for clarity. (c) Au L_{III}-edge FT-EXAFS spectrum for Au@Cd-MOF. (d) TEM image for Au@Cd-MOF sample. No particle can be identified from the image. Scale bar: 10 nm. The arrow between (a) and (d) figures schematically illustrates the preparation procedure of Au@Cd-MOF. Adapted with permission from ref. 58*d*. Copyright 2010, Wiley-VCH Verlag GmbH & Co. KGaA.

(EDS) unambiguously gives Au signals. No Au clusters larger than 1 nm could be found even after the storage of the sample in air for half a year. The Au clusters could be well embedded into the crystalline porous structures of Cd-MOF and the migration or/and aggregation of Au clusters are effectively prevented. It is proposed that the hydrophobic fluoro-coated channels could benefit to embody the Au clusters. XAFS data analyses have demonstrated the presence of Au(0) and the ultrafine Au clusters with an average atom number of 2.5. Moreover, in addition to Au–Au, Au–F or Au–O interactions could also exist in Au@Cd-MOF, as suggested by the Fourier transform magnitude of the EXAFS (FT-EXAFS) spectrum (Fig. 12c).[58d]

4.2 Functional applications

So far, there are four reports on enhanced hydrogen storage on Pt@MOFs or Pd@MOFs based on a spillover mechanism,[20] which we have discussed in the gas storage and separation section. Besides these, the functional applications of metal NPs deposited to MOFs are mainly for catalysis and the catalytic reactions are mostly focused on oxidation of alcohols, hydrogenation reaction, CO oxidation and C–C coupling reaction, *etc*.

4.2.1 Catalytic oxidation of alcohols. The catalytic alcohol oxidation reaction is the most studied reaction of metal NP loaded MOF catalysts thus far (Scheme 1). Kempe and coworkers have shown that Pt@MOF-177 catalyzes the solvent- and base-free oxidation of allylic alcohols at room temperature with air as an oxidant. Cinamyl alcohol and benzyl alcohol and its derivatives are oxidized smoothly under very mild conditions with turnover numbers (TONs) of up to 1000. Unfortunately, the breakdown of the MOF-177 host

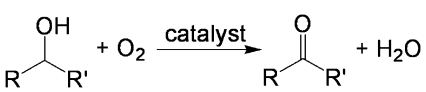

Scheme 1 Catalytic alcohol oxidation reaction.

This journal is © The Royal Society of Chemistry 2011

Downloaded by University of Science and Technology of China on 07/05/2013 04:06:21.
Published on 02 February 2011 on http://pubs.rsc.org | doi:10.1039/C0CC05419D

matrix occurs because H_2O is produced as a byproduct during the reaction.[20b] Fischer and coworkers have employed Ru@MOF-5 as a catalyst for alcohol oxidation at 80 °C. Similarly, MOF-5 also decomposes due to the formation of H_2O during the oxidation reaction.[57d] Ishida *et al.* introduced Au clusters to various MOF supports, which exhibited noticeably higher catalytic activity toward liquid phase aerobic alcohol oxidation even in the absence of base. The authors present two characteristic features based on the experimental results: (i) the selection of MOF supports significantly affected catalytic activity and product selectivity, and (ii) catalytic activity of Au/MOFs was superior to Au/AC (activated carbon) and Au/SiO_2 under base-free conditions. In addition, the selection of suitable MOF supports and the preparation method to obtain small size Au clusters appeared to be the important factors for the catalytic reaction results.[58a] The Au/MIL-101 catalyst reported by Liu *et al.* exhibited very high catalytic activities in liquid-phase aerobic oxidation of a wide range of alcohols, which could even efficiently catalyze the oxidation under ambient conditions in the absence of water or base. Moreover, the catalyst was easily recoverable and could be reused several times without leaching of metals or debasing of activity. The high dispersion of Au NPs and the electron donation effects of aryl rings to the Au NPs within the large cages of the MIL-101 support are assumed to be the main reasons for the observed high activities.[56b] The Au@ZIF-8 exhibits a good conversion of 81% and high selectivity of 98% toward liquid-phase aerobic catalytic oxidation of benzyl alcohol to methyl benzoate. In sharp contrast, Au@ZIF-90 reveals a very weak catalytic activity with a conversion of only 13% and a selectivity drop to 50%. It is proposed that the intercalated Au NPs in ZIF-90 catalyze the oxidation of the nearby imidazolate-2-carboxyaldehyde groups to imidazolate-2-methylcarboxylate in methanol under oxygen pressure. Therefore, the reaction substrates and products are hindered to reach or effectively interact with the encapsulated Au NPs inside the pores and the residual catalyst performance is considered to be due to the accessible Au NPs outside the pores.[57h]

4.2.2 Catalytic hydrogenation reaction. Kaskel and coworkers have demonstrated that Pd/MOF-5 has a higher catalytic activity in styrene hydrogenation than that of Pd/AC, but *cis*-cyclooctene hydrogenation is much slower due to the different activation energy or/and the small pore opening of MOF-5 which limits the accessibility for the substrates (Scheme 2a and b).[20a] The authors point out that the low chemical stability and sensitivity against moisture of MOF-5 host affects the practical applicability. Therefore, they have subsequently developed a Pd/MIL-101 catalyst with high stability in air. Pd/MIL-101 clearly shows the highest activity in the hydrogenation of both styrene and *cis*-cyclooctene compared to Pd/MOF-5, Pd/Norit A and Pd/C with the same Pd loading amount (1 wt%). Moreover, the catalytic stability test of Pd/MIL-101 in the acetylene-ethylene mixture shows its essential advantage over Pd/MOF-5 owing to its stability towards air, moisture and also (reducing) reaction conditions.[54] The Pd NPs supported on MOF-5 were applied for the hydrogenation of ethyl cinnamate with molecular

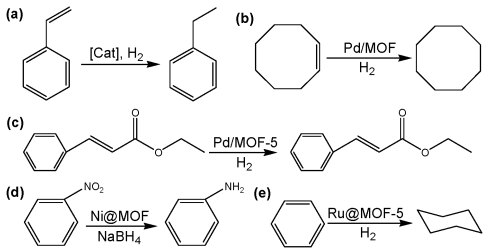

Scheme 2 Catalytic hydrogenation reactions of (a) styrene, (b) *cis*-cyclooctene,(c) ethyl cinnamate, (d) nitrobenzene, and (e) benzene.

hydrogen and showed twice of activity compared to that of commercial Pd/C catalyst with the same Pd content (Scheme 2c). Pd/MOF-5 did not show any loss in activity in repeated runs but a complete loss of micro pore volume was observed.[56a] Kim and coworkers also reported the conversion of styrene to ethylbenzene over Ni/MesoMOF-1 within 4 h under H_2 in methanol at room temperature, indicating that the Ni NPs do not prevent the diffusion of ethylbenzene into the pores. They also showed that the conversion of nitrobenzene to aniline over Ni/MesoMOF-1 was complete within 15 min when $NaBH_4$ was used as hydrogen source in methanol (Scheme 2d). The formation of pure aniline was confirmed even after 3 cycles of the reaction, revealing the stability of the MOF framework.[57g] In addition, the Ru/MOF-5 catalyst showed 25% hydrogenation conversion from benzene to cyclohexane under 3 bar H_2 at 75 °C with intact MOF-5 framework (Scheme 2e).[57d]

4.2.3 Catalytic CO oxidation. We first reported the CO oxidation activity over Au@ZIF-8 having different Au contents (0.5–5 wt%) with 50% conversion ranging from 175 to 225 °C. The activity increases along with the Au loadings till 5 wt% and the high thermal stability of ZIF-8 is considered to be one of the important factors for the observed activity. It is worthy to note that both the ZIF-8 host framework and Au NPs remain stable based on PXRD and TEM examinations under the harsh reaction conditions and even after several runs of reactions. It is assumed that the migration and aggregation of Au NPs are effectively prevented due to the pore structure limitation for them.[58c] Afterwards, Al-Shall *et al.* reported higher CO oxidation activities over Pd/MIL-101. Among Pd loadings of 0.1–4.9 wt%, 2.9 wt% Pd/MIL-101 has the highest activity with 100% conversion at 107 °C. The authors propose that most of the activity comes from the small Pd NPs within 3 nm incorporated in the pores. The catalytic activity for 2 wt% Cu/MIL-101 shows 100% conversion at higher temperature (289 °C). Remarkably, the mixed Pd-Cu catalysts with 2 wt% Cu and 0.5 wt% or 1 wt% Pd show significant enhancement with 100% conversion at 180 °C and 152 °C, respectively probably due to the formation of PdCu nanoalloy.[55b]

4.2.4 Catalytic C–C coupling reaction. The Pd loaded APS-MIL-101 (0.93 wt% Pd) and ED-MIL-101 (0.95 wt% Pd) developed by Hwang *et al.* have considerably high activities toward the Heck reaction at 120 °C (Scheme 3a).[55a] Their activities were comparable with that of a commercial Pd/C catalyst (1.09 wt% Pd) after a certain induction period

Downloaded by University of Science and Technology of China on 07/05/2013 04:06:21.
Published on 02 February 2011 on http://pubs.rsc.org | doi:10.1039/C0CC05419D

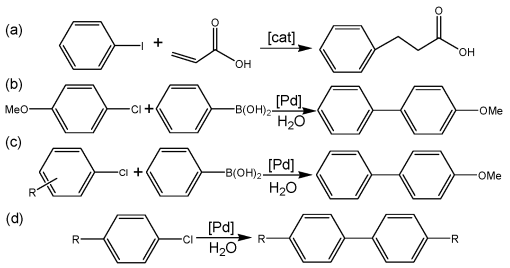

Scheme 3 Catalytic (a) Heck coupling reaction with Pd-based catalysts, (b) Suzuki-Miyaura coupling of 4-chloroanisol with Pd/MIL-101, (c) Suzuki-Miyaura coupling reactions of aryl chlorides over supported Pd catalysts, and (d) Ullmann coupling reactions of aryl chlorides over supported Pd catalysts.

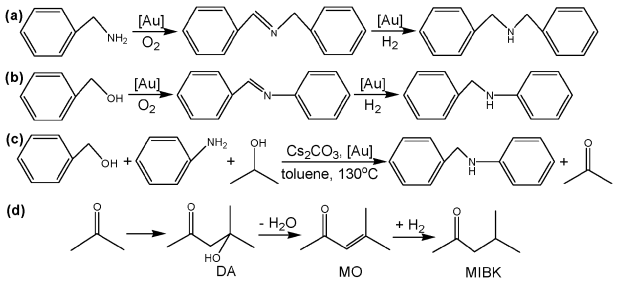

Scheme 4 One-pot synthesis of (a) symmetric secondary amines and (b) unsymmetrical secondary amines. (c) *N*-Alkylation in the presence of 2-propanol and Cs_2CO_3 under N_2 atmosphere. (d) Synthesis of MIBK from acetone and H_2.

(0.5–1 h), probably due to the slow diffusion of reactants to reach accessible metal sites in the pores. Yuan *et al.* have developed Pd/MIL-101 composites for water-mediated coupling reactions of aryl chlorides (Scheme 3b–d).[55c] When 4-chloroanisole was employed as the substrate in the screening of Suzuki-Miyaura coupling reaction over Pd/MIL-101, the addition of tetrabutylammonium bromide (TBAB) significantly enhanced the yield and the highest yield was obtained when the reaction was carried out using NaOMe as a base. High catalytic activities were also observed for Pd/MIL-101 when investigating the scope of aryl chlorides in the Suzuki-Miyaura coupling reaction with phenylboronic acid. In contrast, Pd/C and Pd/ZIF-8 showed lower activities. The authors attributed the higher activity of Pd/MIL-101 over Pd/ZIF-8 to the larger surface area and pore size of MIL-101 as well as the open metal Cr^{3+} centers. It has been found that the existence of reduced Pd^0 is crucial for the activity and the atmosphere in the reaction is also an important impact on the efficiency of the Suzuki-Miyaura coupling process. In addition, the Pd/MIL-101 catalyst gave exceptionally high activity and selectivity for the Ullmann coupling of aryl chlorides in the absence of phenylboronic acid using water as the solvent at a moderate temperature. The catalyst can be readily recovered and reused for 5 cycles of the Ullmann coupling reaction without loss of efficiency. Meanwhile, the Pd NP sizes almost remain and the loss of Pd active sites is demonstrated to be negligible after catalytic reaction.

4.2.5 Other catalytic reactions. The Pd/MOF-5 and Cu/MOF-5 were tested to have moderate activities, respectively for cyclooctene hydrogenation and methanol production from synthesis gas. The MOF-5 framework in Cu/MOF-5 remains stable during the catalysis condition (220 °C, CO/H_2).[57a] Ishida *et al.* prepared Au/MIL-53 (Al) with 1.6 nm of Au NPs, which was able to catalyze one-pot synthesis of secondary amines from primary amines by sequential oxidation/hydrogenation due to the remarkable improvement of hydrogenation efficiency of imines (Scheme 4a and b). In addition, Au/MIL-53 can also promote *N*-alkylation of amines with alcohol to form a secondary amine under N_2 atmosphere without using O_2 and H_2 (Scheme 4c). It was reported that the hydrogenation of imines to amines was significantly enhanced when Au clusters are smaller than 2 nm, leading to high catalytic performance for one-pot, two-step synthesis of secondary amines.[58b] Pan *et al.* have evaluated Pd/MIL-101 as a highly active catalyst for liquid-phase one-step synthesis of methyl isobutyl ketone (MIBK) (Scheme 4d). Results revealed that higher Pd loading led to improved acetone conversion and increased selectivity to 2-propanol but decreased selectivity to MIBK. The 0.11 wt% Pd loading was used as an optimized value and the best performance of 0.11 wt% Pd/MIL-101 obtained at 150 °C gave 90.2% MIBK selectivity at 60% conversion. No efficiency loss of 0.11 wt% Pd/MIL-101 for the MIBK synthesis was observed after 5 cycles of reaction and also the Pd NP sizes as well as MIL-101 framework were mostly retained.[55d]

The three main methods for deposition of metal NPs to porous MOFs have their respective benefits and drawbacks. For example, the pre-grafting of the amino group on unsaturated metal centers and subsequent metal precursor anchoring by a solution method allows better dispersion compared to direct impregnation but it is not straightforward. The gas-phase and solid-grinding infiltration of the precursor into the host MOF is the inclusion of the precursor molecules without competition with solvent molecules whereas only volatile precursors can be used. The metal NPs loaded to porous MOFs as a new class of emerging nanocomposites affords new opportunities to extend functional applications of MOFs, especially in catalysis and hydrogen storage; primary but very promising results have been achieved. However, better understanding and more straightforward characterizations for these nanocomposites (such as, size control and the location of metal NPs, optimization of metal loading amount, *etc.*), still remain as challenging issues and require more efforts in this topic.

5. Porous MOFs as templates/nanoreactors

Porous MOFs with crystalline frameworks and homogeneous pore spaces have provided great opportunities for nanospace chemistry, which allows the formation of new tailor-made materials/arrays with the aid of the specific nanospace as reaction vessels. In some cases, the host framework as hard template could be effectively removed upon completion of the nanospace-confined reaction, leaving the desired inclusion materials/arrays behind.

Li and coworkers have synthesized a thermally stable, 3D Co-based nanoporous MOF, $[Co_3(bpdc)_3(bpy)]\cdot 4DMF\cdot H_2O$ (bpdc = biphenyldicarboxylate, bpy = 4,4′-bipyridine), with

 This journal is © The Royal Society of Chemistry 2011

Downloaded by University of Science and Technology of China on 07/05/2013 04:06:21.
Published on 02 February 2011 on http://pubs.rsc.org | doi:10.1039/C0CC05419D

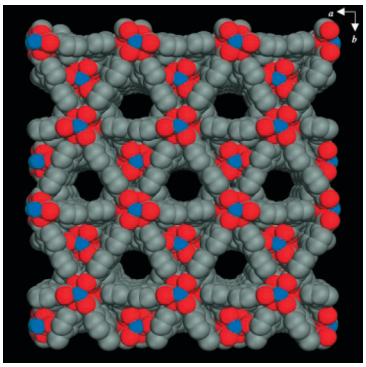

Fig. 13 Top view (001) of the channels in the 3D Co-based MOF showing the window openings. Co (light blue), O (red), N (blue), C (gray). Reproduced with permission from ref. 59. Copyright 2003, Wiley-VCH Verlag GmbH & Co. KGaA.

a nonporous 1D coordination polymer as the starting material, $[Co(bpdc)(H_2O)_2]\cdot H_2O$ (eqn (1)).[59] The 3D Co-based MOF features a 2-fold interpenetrated network and has 1D channels containing large diameter supercages and smaller windows (Fig. 13). The authors have successfully demonstrated the unique potential of the 3D MOF to serve as a "smart" porous host for "ship in bottle" photochemistry and it has outstanding shape selectivity in the photolysis of ortho-methyldibenzylketone (*o*-MeDBK), to give a cage effect of 100% of the α-cleavage products and a high yield of the cyclization product. With the help of the interconversion of such a 3D MOF and its 1D precursor under suitable conditions, a mass balance of 100% is achieved by breaking the 3D framework. The presented 3D MOF not only demonstrated a similar or better performance in sorption and catalysis than some of the most commonly used zeolites (ZSM-5, X, and Y), but it is also the first recyclable nanoporous metal–organic compound whose framework (the bottle) can be completely broken down under mild conditions to allow a full recovery of photochemical products.

$$[Co(bpdc)(H_2O)_2]\cdot H_2O + bpy \underset{H_2O,R.T.}{\overset{DMF,150^\circ C}{\rightleftharpoons}} [Co_3(bpdc)_3(bpy)]\cdot 4DMF\cdot H_2O \quad (1)$$

Kitagawa and coworkers have explored the radical polymerization of styrene in the 1D nanochannels of MOFs and carefully studied the link between reactivity and local dynamic behavior of styrene in the nanochannels by NMR. Studies have indicated that the propagating radicals of polystyrene show living radical nature and styrene reactivity can be determined by the confinement effect in the nanochannels.[60a,b] Following this research line, they have also realized the topotactic selective radical polymerization of divinylbenzenes (DVBs) in 1D channels of porous MOFs to obtain poly(DVBs) with a regulated 1D chain structure bearing pendant vinyl groups (Fig. 14). They have proposed that the prerequisites for this polymerization are an appropriate channel size for the adsorbed monomer and/or framework flexibility to allow monomer adsorption and arrangement.[60c]

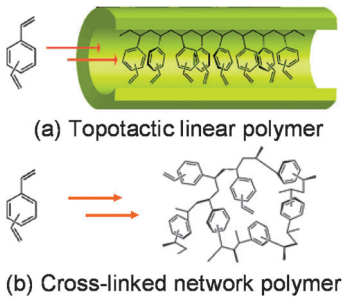

Fig. 14 Schematic illustration for the radical polymerization of divinylbenzenes (DVBs) in (a) 1D channels of porous MOFs to afford a topotactic linear polymer and (b) bulk or solution to yield cross-linked network polymer. Adapted with permission from ref. 60*c*. Copyright 2007, Wiley-VCH Verlag GmbH & Co. KGaA.

In addition, the functionalized pore surface makes porous MOFs have active sites in or on nanochannels. The authors have performed controlled and selective polymerization of substituted acetylenes in 1D specific nanochannels of MOFs with basic carboxylate oxygen atoms as catalytic interaction sites on the pore walls. The polymerization within the porous MOF bearing surface basic carboxylate oxygen atoms exhibits several interesting features: dramatic acceleration of polymerization, no production of trisubstituted benzenes as byproducts, and *trans*-selective polymerization. Results indicate that the strong hydrogen-bonding interaction (acid-base) between the monomers and the channel surface is a key factor to the unique spontaneous polymerization.[60d] With systematic functionalization of a porous MOF by introducing various substituents onto the component organic linker to regulate the radical polymerization of methyl methacrylate (MMA) in the nanochannels, the authors have discovered that the tacticity of the poly(MMA) strongly depends on the number and position of the substituent.[60e] They have also fabricated silica by using tetramethoxysilane as a precursor and a sol–gel reaction inside 1D channels of MOFs without damaging the host structure or depositing the silica particles outside the pores. Interestingly, a drastic decrease of the crystallization temperature for silica was observed because of its minute formation.[60f]

Our group has firstly obtained nanoporous carbon (NPC) with high surface area by using a MOF-5 as the template and furfuryl alcohol (FA) as the carbon precursor.[61a,b] The desolvated MOF-5 was introduced into the FA atmosphere and heated at 150 °C for 2 days, during which FA was polymerized to poly(furfuryl alcohol) (PFA) in the pores of MOF-5. Afterwards, the PFA/MOF-5 composite was allowed to be calcined at 1000 °C in a flowing Ar atmosphere to yield NPC (Fig. 15). The N_2 sorption examinations show that BET surface area and pore volume of the resultant carbon material are 2872 $m^2\ g^{-1}$ and 2.06 $cm^3\ g^{-1}$, respectively. The carbonization temperature is critical for the structural evolution of the resultant carbon and carbonization at 800 °C gives rise to much lower BET surface area (417 $m^2\ g^{-1}$) and pore volume (0.63 $cm^3\ g^{-1}$). The H_2 uptake for the carbon obtained at 1000 °C is as high as 2.6 wt% at 1 atm, twice of that of MOF-5. In addition, the as-synthesized porous carbon material exhibits excellent electrochemical performance as an electrode material for electrochemical double-layered capacitor

Downloaded by University of Science and Technology of China on 07/05/2013 04:06:21.
Published on 02 February 2011 on http://pubs.rsc.org | doi:10.1039/C0CC05419D

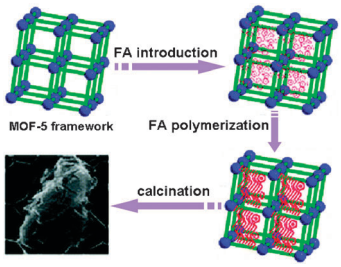

Fig. 15 The formation procedure for the MOF-5 templated nanoporous carbon. Adapted with permission from ref. 61*a*. Copyright 2008, American Chemical Society.

(EDLC). A two electrode carbon-based capacitor (electrolyte, 1.0 M H_2SO_4) cycling potentiodynamically between −0.5 and 0.5 V behaves like an ideal capacitor showing rectangular voltammograms without any redox peaks. Typical triangular shapes of galvanostatic charge-discharge curves also confirm good capacitive properties of NPC. The specific capacitance is maintained as high as 258 F g^{-1} even at a current density of 250 mA g^{-1}.[61*a*] Besides FA vapor introduction method, we have recently verified that incipient wetness impregnation (IMP) method also works well. With similar procedures except for FA introduced by IMP method, NPC materials have been obtained by carbonizing at the temperatures from 530 to 1000 °C with surface areas ranging from 1140 to 3040 m^2 g^{-1}. All the samples have pore size distributions centered at ~3.9 nm. As electrode materials for supercapacitor, the samples obtained at the temperatures higher than 600 °C display the ideal capacitor behaviors and give rise to almost constant specific capacitance (above 100 F g^{-1} at 5 mV s^{-1}) at various sweep rates, which is associated with their mesoporous characteristics. However, the sample with the highest BET surface area (3040 m^2 g^{-1}) obtained by carbonizing at 530 °C gives a unusually low capacitance (12 F g^{-1} at 5 mV s^{-1}), probably due to the poor conductivity of the carbon material.[61*b*] Hu and Yuan and their coworkers have also prepared porous carbon with MOF template with similar synthsis route.[61*c*,*d*] In addition, Uemura *et al.* have also reported a template synthesis route to fabricate a porous polypyrrole (PPy) by oxidative polymerization of pyrrole (Py) in the 3D channels of HKUST-1 and subsequent template removal.[61*e*]

Allendorf and coworkers have confined $NaAlH_4$ into the pores of HKUST-1 as a template to investigate the H_2 desorption kinetics. Studies show that 4 wt% $NaAlH_4$ loaded HKUST-1 has very different H_2 desorption behavior from bulk $NaAlH_4$, in which multiple chemical or/and physical processes are involved. Neat $NaAlH_4$ desorbs 70% of its H_2 at $T \approx 250$ °C. In contrast, $NaAlH_4$ confined within the MOF pores decomposes at ~100 °C lower than bulk $NaAlH_4$. The MOF host matrix is not decomposed during $NaAlH_4$ decomposition based on PXRD investigations. Results suggest that nanoscale effects result from a combination of reduced size and the local chemical environment confining the clusters.[62] In addition, Li *et al.* have synthesized MOF-confined NH_3BH_3 system by the infusion method recently. The selected microporous MOF with 1D tubular channels of size of ~6 Å (larger than NH_3BH_3) has very high thermal stability and also unsaturated metal Y^{3+} sites upon heat pretreatment. Neat NH_3BH_3 has two-step decomposition at ~150 °C, producing a large amount of hydrogen, mixed with the unexpected byproducts borazine, ammonia, and diborane. In contrast, the decomposition of NH_3BH_3 inside MOF started at only ~50 °C and the peak temperature of NH_3BH_3 decomposition was shifted to 84 °C (compared with 114 °C for neat NH_3BH_3). This is the first reported achievement of such a big decrease (30 °C) in the decomposition temperature, confirming the nanoconfinement effect. Furthermore, no volatile products were found during the decomposition process. It is assumed that the synergistic effect of nanoconfinement and metallic catalysis, where the small pore size of MOF strongly confined NH_3BH_3 to lower its decomposition temperature much and the catalytic unsaturated Y^{3+} sites in MOF interacted with NH_3BH_3 to completely prevent the formation of ammonia.[63]

Oh and coworkers reported the formation of hexagonal tubes and rings of MOFs (or called as coordination polymers) by the simple solvothermal reaction of metal ions and carboxy-functionized building blocks. As shown in Fig. 16, the hexagonal lumps or disks as initial products were formed at a very early stage before thermal treatment based on the amounts of $Zn(OAc)_2$ used. After thermal treatment, new MOFs began to grow on the lateral facets of the initial hexagonal lumps/disks, which act as the template and are gradually dissolved. The initial MOF templates become thinner and finally disappear, leaving uniform hexagonal tubes/rings. Based on shape-evolved SEM observations, the authors have proposed a concurrent two-step process of self-template-directed growth mechanism, involving secondary surrounding MOF growth and followed by initial supporting template dissolving. Interestingly, the obtained atypically shaped MOF can be calcined as templates to generate pure bulk ZnO with similar shape (nanoring).[64*a*] Afterwards, they have again demonstrated that the original morphology of the

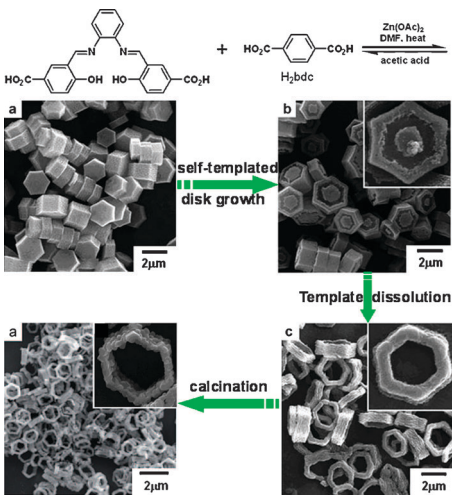

Fig. 16 SEM images for the shape evolution process of the MOF. (a) The MOF lumps/disks formed in the early stage. (b, c) The MOF microstructures at the later stages upon heat treatment. (d) The ZnO rings formed after calcination. Insets: high-magnification images. Adapted with permission from ref. 64*a*. Copyright 2009, Wiley-VCH Verlag GmbH & Co. KGaA.

 This journal is © The Royal Society of Chemistry 2011

Downloaded by University of Science and Technology of China on 07/05/2013 04:06:21.
Published on 02 February 2011 on http://pubs.rsc.org | doi:10.1039/C0CC05419D

MOF template can be maintained in the resulting In_2O_3 products by the calcination of hexagonal rod-shaped In-MOF microparticles. It is found that the composition and porosity of the MOF precursor also affect the resultant In_2O_3 structure. Non-hollow and hollow-structured In_2O_3 particles were generated from the calcination of porous and non-porous MOFs, respectively.[64b] Our group have developed a MOF-based route for preparing agglomerated Co_3O_4 NPs which involves the processes of converting metal oxide subunits in MOF into primary metal oxide NPs and subsequently agglomerating into the secondary NPs. The as-prepared Co_3O_4 from the porous Co-MOF template[65a] shows an agglomerated secondary structure with an average diameter of $\sim$250 nm comprised of small primary Co_3O_4 particles with a size of about 25 nm. The resultant nanostructured Co_3O_4 as electrode materials for lithium ion battery (LIB) presents a reversible capacity of 965 mA·h g^{-1} (86% of initial capacity) beyond 50 cycles at a current density of 50 mA g^{-1}. The excellent electrochemical performance and the facile preparation suggest practical use of agglomerated Co_3O_4 electrodes in LIB.[65b] By pre-introducing Pt(II) precursor into pores of MOF-5, ZnO-supported Pt NPs have been synthesized by taking advantage of the ZnO subunits in MOF-5 *via* heat treatment. The sizes of Pt NPs can be tuned by changing the concentration of Pt(II) precursor and the resultant Pt/ZnO nanocomposites displayed higher catalytic activities in CO oxidation than conventional Pt/ZnO catalyst.[65c]

The molecules confined in nanospace exhibit unique properties that are not observed in the corresponding bulk state. The highly tailorable pores/channels in MOFs endow them broad applications as nanoreactor or template to yield new materials with specific arrangement of molecules and functions. The potentials and attractiveness of this topic are undoubted although the reports are still limited currently. It is predictable that the "nanoconfinement effect" of porous MOFs will play important roles in materials science in near future.

6. Conclusions

Porous MOFs are emerging as powerful platforms for many incredible functional applications. The highly porous structure, chemical versatility and structural tailorability are the main characteristics and merits of porous MOFs that place them at the forefront of materials science and the development of porous MOFs also proceeds at an extraordinary pace.[2] This feature article has mainly demonstrated that porous MOFs open the door to the following relatively new topics in the last five years: chromatographic separation, (gas-phase) heterogeneous catalysis, as supports/host matrices for small metal NPs, and as templates/nanoreactors for other new material syntheses. These developments are still in their early stages, nevertheless, great potential is possible. However, it is noteworthy that the current studies are mostly focused on a couple of "star" MOFs which are stable and readily reproducible or commercially available. Practical large-scale synthetic methods to afford more alternative chemically and thermally stable and cost-acceptable porous MOFs are urgently required. Moreover, the interdisciplinary application studies ask for the extensive collaborations among chemists and materials scientists in or out of MOF synthetic chemistry field to better understand the relationships between structure and performance. With sustained research efforts towards these challenges, we have every reason to believe that more applications will continuously emerge and porous MOFs should possess a very bright future.

MOF abbreviations used often

MOF-5	$Zn_4O(BDC)_3\cdot(DMF)_8(C_6H_5Cl)$[66]
MOF-177	$Zn_4O(BTC)_2\cdot(DEF)_{15}\cdot(H_2O)_3$[67]
MIL-101	$Cr_3F(H_2O)_2(BDC)_3\cdot nH_2O$ ($n \approx 25$)[5a]
MIL-47	$V(OH)(BDC)\cdot(BDC)_x$ ($x \approx 0.75$)[68]
MIL-53(Al)	$Al(OH)(BDC)\cdot(BDC)_{0.70}$[69]
HKUST-1	$Cu(BTC)(H_2O)_3$[70]
ZIF-8	$Zn(imidazolate)_2\cdot(DMF)\cdot(H_2O)_3$[71]
MIL-100(Al)	$Al_3O(OH)(H_2O)_2(BTC)_2\cdot nH_2O$[72]
BDC	1,4-benzenedicarboxylate
BTC	benzene-1,3,5-tricarboxylate

Acknowledgements

We are grateful to AIST and JSPS for financial support. H.L.J. thanks JSPS for a postdoctoral fellowship.

Notes and references

1 (*a*) B. F. Hoskins and R. Robson, *J. Am. Chem. Soc.*, 1989, **111**, 5962–5964; (*b*) B. F. Hoskins and R. Robson, *J. Am. Chem. Soc.*, 1990, **112**, 1546–1554.
2 (*a*) S. Kitagawa, R. Kitaura and S. Noro, *Angew. Chem., Int. Ed.*, 2004, **43**, 2334–2375; (*b*) G. Férey, *Chem. Soc. Rev.*, 2008, **37**, 191–214; (*c*) J. R. Long and O. M. Yaghi, *Chem. Soc. Rev.*, 2009, **38**, 1213–1214 and mentioned references therein.
3 (*a*) M. Eddaoudi, J. Kim, N. Rosi, D. Vodak, J. Wachter, M. O'Keeffe and O. M. Yaghi, *Science*, 2002, **295**, 469–472; (*b*) W. J. Zhuang, S. Ma, X.-S. Wang, D. Yuan, J.-R. Li, D. Zhao and H.-C. Zhou, *Chem. Commun.*, 2010, **46**, 5223–5225; (*c*) L. Ma and W. Lin, *J. Am. Chem. Soc.*, 2008, **130**, 13834–13835; (*d*) O. Shekhah, H. Wang, M. Paradinas, C. Ocal, B. Schüpbach, A. Terfort, D. Zacher, R. A. Fischer and C. Wöll, *Nat. Mater.*, 2009, **8**, 481–484; (*e*) Y. K. Park, S. B. Choi, H. Kim, K. Kim, B.-H. Won, K. Choi, J.-S. Choi, W.-S. Ahn, N. Won, S. Kim, D. H. Jung, S.-H. Choi, G.-H. Kim, S.-S. Cha, Y. H. Jhon, J. K. Yang and J. Kim, *Angew. Chem., Int. Ed.*, 2007, **46**, 8230–8233; (*f*) O. K. Farha, C. D. Malliakas, M. G. Kanatzidis and J. T. Hupp, *J. Am. Chem. Soc.*, 2010, **132**, 950–952; (*g*) H.-L. Jiang, Y. Tastu, Z.-H. Lu and Q. Xu, *J. Am. Chem. Soc.*, 2010, **132**, 5586–5587.
4 Z. Wang and S. M. Cohen, *Chem. Soc. Rev.*, 2009, **38**, 1315–1329.
5 (*a*) G. Férey, C. Mellot-Draznieks, C. Serre, F. Millange, J. Dutour, S. Surblé and I. Margiolaki, *Science*, 2005, **309**, 2040–2042; (*b*) H. Furukawa, N. Ko, Y. B. Go, N. Aratani, S. B. Choi, E. Choi, A. O. Yazaydin, R. Q. Snurr, M. O'Keeffe, J. Kim and O. M. Yaghi, *Science*, 2010, **329**, 424–428.
6 (*a*) B. Moulton and M. J. Zaworotko, *Chem. Rev.*, 2001, **101**, 1629–1658; (*b*) M. Du, Z.-H. Zhang, L.-F. Tang, X.-G. Wang, X.-J. Zhao and S. R. Batten, *Chem.–Eur. J.*, 2007, **13**, 2578; (*c*) R.-Q. Zou, R.-Q. Zhong, M. Du, T. Kiyobayashia and Q. Xu, *Chem. Commun.*, 2007, 2467–2469; (*d*) S. Natarajan and P. Mahata, *Chem. Soc. Rev.*, 2009, **38**, 2304–2318; (*e*) H.-L. Jiang, B. Liu and Q. Xu, *Cryst. Growth Des.*, 2010, **10**, 806–811; (*f*) H.-L. Jiang and Q. Xu, *CrystEngComm*, 2010, **12**, 3815–3819; (*g*) B.-X. Dong, X.-J. Gu and Q. Xu, *Dalton Trans.*, 2010, **39**, 5683–5687; (*h*) R.-Q. Zhong, R.-Q. Zou, M. Du, N. Takeichi and Q. Xu, *CrystEngComm*, 2008, **10**, 1175–1179; (*i*) M. J. Prakash and M. S. Lah, *Chem. Commun.*, 2009, 3326–3341; (*j*) Y.-Q. Lan, X.-L. Wang, S.-L. Li, Z.-M. Su, K.-Z. Shao and E.-B. Wang,

View Article Online

Downloaded by University of Science and Technology of China on 07/05/2013 04:06:21.
Published on 02 February 2011 on http://pubs.rsc.org | doi:10.1039/C0CC05419D

Chem. Commun., 2007, 4863–4865; (*k*) C. Mellot-Draznieks, C. Serre, S. Surblé, N. Audebrand and G. Férey, *J. Am. Chem. Soc.*, 2005, **127**, 16273–16278.

7 (*a*) M. Kurmoo, *Chem. Soc. Rev.*, 2009, **38**, 1353–1379; (*b*) Q. Xu, R.-Q. Zou, R.-Q. Zhong, C. Kachi-Terajima and S. Takamizawa, *Cryst. Growth Des.*, 2008, **8**, 2458–2463; (*c*) R.-Q. Zhong, R.-Q. Zou, M. Du, T. Yamada, G. Maruta, S. Takeda and Q. Xu, *Dalton Trans.*, 2008, 2346–2354; (*d*) R.-Q. Zhong, R.-Q. Zou, M. Du, T. Yamada, G. Maruta, S. Takeda, J. Li and Q. Xu, *CrystEngComm*, 2010, **12**, 677–681; (*e*) R.-Q. Zhong, R.-Q. Zou, M. Du, L. Jiang, T. Yamada, G. Maruta, S. Takeda and Q. Xu, *CrystEngComm*, 2008, **10**, 605–613; (*f*) L. Hou, W.-X. Zhang, J.-P. Zhang, W. Xue, Y.-B. Zhang and X.-M. Chen, *Chem. Commun.*, 2010, **46**, 6311–6313.

8 (*a*) M. D. Allendorf, C. A. Bauer, R. K. Bhakta and R. J. T. Houk, *Chem. Soc. Rev.*, 2009, **38**, 1330–1352; (*b*) R.-Q. Zou, R.-Q. Zhong, M. Du, D. S. Pandey and Q. Xu, *Cryst. Growth Des.*, 2008, **8**, 452–459; (*c*) R.-Q. Zou, Y. Yamada and Q. Xu, *Microporous Mesoporous Mater.*, 2006, **91**, 233–237; (*d*) R.-Q. Zou, R.-Q. Zhong, L. Jiang, Y. Yamada, N. Kuriyama and Q. Xu, *Chem.–Asian J.*, 2006, **1**, 536–543; (*e*) R.-Q. Zhong, R.-Q. Zou and Q. Xu, *Microporous Mesoporous Mater.*, 2007, **102**, 122–127; (*f*) J. Xu, Z.-S. Bai, M.-S. Chen, Z. Su, S.-S. Chen and W.-Y. Sun, *CrystEngComm*, 2009, **11**, 2728–2733.

9 (*a*) M. Fujita, Y. J. Kwon, S. Washizu and K. Ogura, *J. Am. Chem. Soc.*, 1994, **116**, 1151–1152; (*b*) J. S. Seo, D. Whang, H. Lee, S. I. Jun, J. Oh, Y. J. Jeon and K. Kim, *Nature*, 2000, **404**, 982–986; (*c*) D. Farrusseng, S. Aguado and C. Pinel, *Angew. Chem., Int. Ed.*, 2009, **48**, 7502–7513; (*d*) L. Ma, C. Abney and W. Lin, *Chem. Soc. Rev.*, 2009, **38**, 1248–1256; (*e*) J. Y. Lee, O. K. Farha, J. Roberts, K. A. Scheidt, S. T. Nguyen and J. T. Hupp, *Chem. Soc. Rev.*, 2009, **38**, 1450–1459; (*f*) A. Corma, H. García and F. X. Llabrés i Xamena, *Chem. Rev.*, 2010, **110**, 4606–4655.

10 (*a*) J. Y. Lee, L. Pan, S. P. Kelly, J. Jagiello, T. J. Emge and J. Li, *Adv. Mater.*, 2005, **17**, 2703–2706; (*b*) R.-Q. Zou, L. Jiang, H. Senoh, N. Takeichi and Q. Xu, *Chem. Commun.*, 2005, 3526–3528; (*c*) L. J. Murray, M. Dincă and J. R. Long, *Chem. Soc. Rev.*, 2009, **38**, 1294–1314; (*d*) J.-R. Li, R. J. Kuppler and H.-C. Zhou, *Chem. Soc. Rev.*, 2009, **38**, 1477–1504; (*e*) S. Ma and H.-C. Zhou, *Chem. Commun.*, 2010, **46**, 44–53; (*f*) H.-L. Jiang, N. Tsumori and Q. Xu, *Inorg. Chem.*, 2010, **49**, 10001–10006; (*g*) S.-S. Chen, M. Chen, S. Takamizawa, M.-S. Chen, Z. Su and W.-Y. Sun, *Chem. Commun.*, 2011, **47**, 752–754.

11 (*a*) T. Uemura, N. Yanai and S. Kitagawa, *Chem. Soc. Rev.*, 2009, **38**, 1228–1236; (*b*) M. Meilikhov, K. Yusenko, D. Esken, S. Turner, G. Van Tendeloo and R. A. Fischer, *Eur. J. Inorg. Chem.*, 2010, 3701–3714; (*c*) H. L. Jiang, T. Akita, T. Ishida, M. Haruta and Q. Xu, *J. Am. Chem. Soc.*, 2011, DOI: 10.1021/ja1099006.

12 (*a*) D. Zacher, O. Shekhah, C. Wöll and R. A. Fischer, *Chem. Soc. Rev.*, 2009, **38**, 1418–1429; (*b*) R. Makiura, S. Motoyama, Y. Umemura, H. Yamanaka, O. Sakata and H. Kitagawa, *Nat. Mater.*, 2010, **9**, 565–571.

13 (*a*) B. Chen, S. Xiang and G. Qian, *Acc. Chem. Res.*, 2010, **43**, 1115–1124; (*b*) M. Sadakiyo, T. Yamada and H. Kitagawa, *J. Am. Chem. Soc.*, 2009, **131**, 9906–9907; (*c*) S. Bureekaew, S. Horike, M. Higuchi, M. Mizuno, T. Kawamura, D. Tanaka, N. Yanai and S. Kitagawa, *Nat. Mater.*, 2009, **8**, 831–836; (*d*) J. A. Hurd, R. Vaidhyanathan, V. Thangadurai, C. I. Ratcliffe, I. L. Moudrakovski and G. K. H. Shimizu, *Nat. Chem.*, 2009, **1**, 705–710.

14 (*a*) P. Horcajada, C. Serre, M. Vallet-Regí, M. Sebban, F. Taulelle and G. Férey, *Angew. Chem., Int. Ed.*, 2006, **45**, 5974–5978; (*b*) K. M. L. Taylor-Pashow, J. D. Rocca, Z. Xie, S. Tran and W. Lin, *J. Am. Chem. Soc.*, 2009, **131**, 14261–14263.

15 (*a*) S. Horike, S. Shimomura and S. Kitagawa, *Nat. Chem.*, 2009, **1**, 695–704; (*b*) Y.-G. Huang, F.-L. Jiang and M.-C. Hong, *Coord. Chem. Rev.*, 2009, **253**, 2814–2834; (*c*) S. Qiu and G. Zhu, *Coord. Chem. Rev.*, 2009, **253**, 2891–2911; (*d*) X. Lin, J. Jia, P. Hubberstey, M. Schröder and N. R. Champness, *CrystEngComm*, 2007, **9**, 438–448; (*e*) R. J. Kuppler, D. J. Timmons, Q.-R. Fang, J.-R. Li, T. A. Makal, M. D. Young, D. Yuan, D. Zhao, W. Zhuang and H.-C. Zhou, *Coord. Chem. Rev.*, 2009, **253**, 3042–3066.

16 N. L. Rosi, J. Eckert, M. Eddaoudi, D. T. Vodak, J. Kim, M. O'Keefe and O. M. Yaghi, *Science*, 2003, **300**, 1127–1129.

17 X. Gu, Z.-H. Lu and Q. Xu, *Chem. Commun.*, 2010, **46**, 7400–7402.

18 (*a*) S. S. Kaye, A. Dailly, O. M. Yaghi and J. R. Long, *J. Am. Chem. Soc.*, 2007, **129**, 14176–14177; (*b*) H. Furukawa, M. A. Millerb and O. M. Yaghi, *J. Mater. Chem.*, 2007, **17**, 3197–3204; (*c*) D. Saha, Z. Wei and S. Deng, *Int. J. Hydrogen Energy*, 2008, **33**, 7479–7488.

19 (*a*) Y. Li and R. T. Yang, *J. Am. Chem. Soc.*, 2006, **128**, 726–727; (*b*) Y. Li and R. T. Yang, *J. Am. Chem. Soc.*, 2006, **128**, 8136–8137.

20 (*a*) M. Sabo, A. Henschel, H. Fröde, E. Klemm and S. Kaskel, *J. Mater. Chem.*, 2007, **17**, 3827–3832; (*b*) S. Proch, J. Herrmannsdörfer, R. Kempe, C. Kern, A. Jess, L. Seyfarth and J. Senker, *Chem.–Eur. J.*, 2008, **14**, 8204–8212; (*c*) Y. E. Cheon and M. P. Suh, *Angew. Chem., Int. Ed.*, 2009, **48**, 2899–2903; (*d*) C. Zlotea, R. Campesi, F. Cuevas, E. Leroy, P. Dibandjo, C. Volkringer, T. Loiseau, F. Férey and M. Latroche, *J. Am. Chem. Soc.*, 2010, **132**, 2991–2997.

21 (*a*) S. S. Han and W. A. Goddard III, *J. Am. Chem. Soc.*, 2007, **129**, 8422–8423; (*b*) A. Blomqvist, C. M. Araujo, P. Srepusharawoot and R. Ahuja, *Proc. Natl. Acad. Sci. U. S. A.*, 2007, **104**, 20173–20176; (*c*) P. Dalach, H. Frost, R. Q. Snurr and D. E. Ellis, *J. Phys. Chem. C*, 2008, **112**, 9278–9284; (*d*) K. L. Mulfort and J. T. Hupp, *J. Am. Chem. Soc.*, 2007, **129**, 9604–9605; (*e*) K. L. Mulfort and J. T. Hupp, *Inorg. Chem.*, 2008, **47**, 7936–7938; (*f*) S. Yang, X. Lin, A. J. Blake, G. S. Walker, P. Hubberstey, N. R. Champness and M. Schröder, *Nat. Chem.*, 2009, **1**, 487–493.

22 (*a*) A. P. Nelson, O. K. Farha, K. L. Mulfort and J. T. Hupp, *J. Am. Chem. Soc.*, 2009, **131**, 458–460; (*b*) L. Ma, A. Jin, Z. Xie and W. Lin, *Angew. Chem., Int. Ed.*, 2009, **48**, 9905–9908; (*c*) Z. Wang, K. K. Tanabe and S. M. Cohen, *Chem.–Eur. J.*, 2010, **16**, 212–217.

23 (*a*) A. R. Millward and O. M. Yaghi, *J. Am. Chem. Soc.*, 2005, **127**, 17998–17999; (*b*) P. L. Llewellyn, S. Bourrely, C. Serre, A. Vimont, M. Daturi, L. Hamon, G. D. Weireld, J.-S. Chang, D.-Y. Hong, Y. K. Hwang, S. H. Jhung and G. Férey, *Langmuir*, 2008, **24**, 7245–7250.

24 M. Kondo, T. Yoshitomi, K. Seki, H. Matsuzaka and S. Kitagawa, *Angew. Chem., Int. Ed. Engl.*, 1997, **36**, 1725–1727.

25 S. Ma, D. Sun, J. M. Simmons, C. D. Collier, D. Yuan and H.-C. Zhou, *J. Am. Chem. Soc.*, 2008, **130**, 1012–1016.

26 (*a*) Y.-S. Bae, O. K. Farha, A. M. Spokoyny, C. A. Mirkin, J. T. Hupp and R. Q. Snurr, *Chem. Commun.*, 2008, 4135–4137; (*b*) H.-S. Choi and M. P. Suh, *Angew. Chem., Int. Ed.*, 2009, **48**, 6865–6869; (*c*) R. Vaidhyanathan, S. S. Iremonger, G. K. H. Shimizu, P. G. Boyd, S. Alavi and T. K. Woo, *Science*, 2010, **330**, 650–653; (*d*) J. An, S. J. Geib and N. L. Rosi, *J. Am. Chem. Soc.*, 2010, **132**, 38–39; (*e*) Y. Inubushi, S. Horike, T. Fukushima, G. Akiyama, R. Matsuda and S. Kitagawa, *Chem. Commun.*, 2010, **46**, 9229–9231; (*f*) H. Wu, R. S. Reali, D. A. Smith, M. C. Trachtenberg and J. Li, *Chem.–Eur. J.*, 2010, **16**, 13951–13954; (*g*) Y.-X. Tan, F. Wang, Y. Kang and J. Zhang, *Chem. Commun.*, 2011, **47**, 770–772.

27 (*a*) B. Xiao, P. J. Byrne, P. S. Wheatley, D. S. Wragg, X. Zhao, A. J. Fletcher, K. M. Thomas, L. Peters, J. S. O. Evans, J. E. Warren, W. Zhou and R. E. Morris, *Nat. Chem.*, 2009, **1**, 289–294; (*b*) D. Saha, Z. Bao, F. Jia and S. Deng, *Environ. Sci. Technol.*, 2010, **44**, 1820–1826; (*c*) S. Shimomura, M. Higuchi, R. Matsuda, K. Yoneda, Y. Hijikata, Y. Kubota, Y. Mita, J. Kim, M. Takata and S. Kitagawa, *Nat. Chem.*, 2010, **2**, 633–637.

28 (*a*) Y. Y. Liu, Z. F. Ng, E. A. Khan, H. K. Jeong, C. B. Ching and Z. P. Lai, *Microporous Mesoporous Mater.*, 2009, **118**, 296–301; (*b*) Y. Yoo, Z. P. Lai and H. K. Jeong, *Microporous Mesoporous Mater.*, 2009, **123**, 100–106; (*c*) H. Guo, G. Zhu, I. J. Hewitt and S. L. Qiu, *J. Am. Chem. Soc.*, 2009, **131**, 1646–1647; (*d*) R. Ranjan and M. Tsapatsis, *Chem. Mater.*, 2009, **21**, 4920–4924; (*e*) H. Bux, F. Liang, Y. Li, J. Cravillon, M. Wiebcke and J. Caro, *J. Am. Chem. Soc.*, 2009, **131**, 16000–16001; (*f*) Y.-S. Li, F.-Y. Liang, H. Bux, A. Feldhoff, W.-S. Yang and J. Caro, *Angew. Chem. Int. Ed.*, 2010, **49**, 548–551; (*g*) A. Huang, W. Dou and J. Caro, *J. Am. Chem. Soc.*, 2010, **132**, 15562–15564; (*h*) A. Huang, H. Bux, F. Steinbach and J. Caro, *Angew. Chem., Int. Ed.*, 2010, **49**, 4958–4961; (*i*) S. R. Venna and M. A. Carreon, *J. Am. Chem. Soc.*, 2010, **132**, 76–78.

 This journal is © The Royal Society of Chemistry 2011

View Article Online

Downloaded by University of Science and Technology of China on 07/05/2013 04:06:21.
Published on 02 February 2011 on http://pubs.rsc.org | doi:10.1039/C0CC05419D

29 (*a*) K. Li, D. H. Olson, J. Seidel, T. J. Emge, H. Gong, H. Zeng and J. Li, *J. Am. Chem. Soc.*, 2009, **131**, 10368–10369; (*b*) L. Pan, D. H. Olson, L. R. Ciemnolonski, R. Heddy and J. Li, *Angew. Chem., Int. Ed.*, 2006, **45**, 616–619; (*c*) J. Y. Lee, D. H. Olson, L. Pan, T. J. Emge and J. Li, *Adv. Funct. Mater.*, 2007, **17**, 1255–1262.

30 (*a*) R. Xiong, X. You, B. F. Abrahams, Z. Xue and C. M. Che, *Angew. Chem., Int. Ed.*, 2001, **40**, 4422–4425; (*b*) O. R. Evans, H. L. Ngo and W. Lin, *J. Am. Chem. Soc.*, 2001, **123**, 10395–10396; (*c*) R. Vaidhyanathan, D. Bradshaw, J. N. Rebilly, J. P. Barrio, J. A. Gould, N. G. Berry and M. J. Rosseinsky, *Angew. Chem., Int. Ed.*, 2006, **45**, 6495–6499; (*d*) K. A. Cychosz, R. Ahmad and A. J. Matzger, *Chem. Sci.*, 2010, **1**, 293–302; (*e*) G. Xu, X. Zhang, P. Guo, C. Pan, H. Zhang and C. Wang, *J. Am. Chem. Soc.*, 2010, **132**, 3656–3657; (*f*) T. Liu, Y. Liu, W. Xuan and Y. Cui, *Angew. Chem. Int. Ed.*, 2010, **49**, 4121–4124.

31 T. Cserhàti and K. Valkó, *Chromatographic Determination of Molecular Interactions: Applications in Biochemistry, Chemistry and Biophysics*, CRC Press, Ann Arbor, 1994.

32 B. Chen, C. Liang, J. Yang, D. S. Contreras, Y. L. Clancy, E. B. Lobkovsky, O. M. Yaghi and S. Dai, *Angew. Chem., Int. Ed.*, 2006, **45**, 1390–1393.

33 (*a*) D. N. Dybtsev, A. L. Nuzhdin, H. Chun, K. P. Bryliakov, E. P. Talsi, V. P. Fedin and K. Kim, *Angew. Chem., Int. Ed.*, 2006, **45**, 916–920; (*b*) A. L. Nuzhdin, D. N. Dybtsev, K. P. Bryliakov, E. P. Talsi and V. P. Fedin, *J. Am. Chem. Soc.*, 2007, **129**, 12958–12959.

34 (*a*) D. N. Dybstev, H. Chun and K. Kim, *Angew. Chem., Int. Ed.*, 2004, **43**, 5033–5036; (*b*) P. S. Bárcia, F. Zapata, J. A. C. Silva, A. E. Rodrigues and B. Chen, *J. Phys. Chem. B*, 2007, **111**, 6101–6103.

35 J. W. Yoon, S. H. Jhung, Y. K. Hwang, S. M. Humphrey, P. T. Wood and J.-S. Chang, *Adv. Mater.*, 2007, **19**, 1830–1834.

36 (*a*) L. Alaerts, C. E. A. Kirschhock, M. Maes, M. A. van der Veen, V. Finsy, A. Depla, J. A. Martens, G. V. Baron, P. A. Jacobs, J. E. M. Denayer and D. E. De Vos, *Angew. Chem., Int. Ed.*, 2007, **46**, 4293–4297; (*b*) L. Alaerts, M. Maes, P. A. Jacobs, J. F. M. Denayer and D. E. De Vos, *Phys. Chem. Chem. Phys.*, 2008, **10**, 2979–2985; (*c*) L. Alaerts, M. Maes, L. Giebeler, P. A. Jacobs, J. A. Martens, J. F. M. Denayer, C. E. A. Kirschhock and D. E. De Vos, *J. Am. Chem. Soc.*, 2008, **130**, 14170–14178; (*d*) L. Alaerts, M. Maes, M. A. van der Veen, P. A. Jacobs and D. E. De Vos, *Phys. Chem. Chem. Phys.*, 2009, **11**, 2903–2911; (*e*) M. Maes, F. Vermoortele, L. Alaerts, S. Couck, C. E. A. Kirschhock, J. F. M. Denayer and D. E. De Vos, *J. Am. Chem. Soc.*, 2010, **132**, 15277–15285; (*f*) M. Maes, L. Alaerts, F. Vermoortele, R. Ameloot, S. Couck, V. Finsy, J. F. M. Denayer and D. E. De Vos, *J. Am. Chem. Soc.*, 2010, **132**, 2284–2292; (*g*) R. Ameloot, A. Liekens, L. Alaerts, M. Maes, A. Galarneau, B. Coq, G. Desmet, B. F. Sels, J. F. M. Denayer and D. E. De Vos, *Eur. J. Inorg. Chem.*, 2010, 3735–3738.

37 (*a*) V. Finsy, H. Verelst, L. Alaerts, D. E. De Vos, P. A. Jacobs, G. V. Baron and J. F. M. Denayer, *J. Am. Chem. Soc.*, 2008, **130**, 7110–7118; (*b*) V. Finsy, C. E. A. Kirschhock, G. Vedts, M. Maes, L. Alaerts, D. E. De Vos, G. V. Baron and J. F. M. Denayer, *Chem.–Eur. J.*, 2009, **15**, 7724–7731; (*c*) V. Finsy, S. Calero, E. Garcíí-Pérez, P. J. Merkling, G. Vedts, D. E. De Vos, G. V. Baron and J. F. M. Denayer, *Phys. Chem. Chem. Phys.*, 2009, **11**, 3515–3521.

38 (*a*) Z.-Y. Gu and X.-P. Yan, *Angew. Chem., Int. Ed.*, 2010, **49**, 1477–1480; (*b*) N. Chang, Z.-Y. Gu and X.-P. Yan, *J. Am. Chem. Soc.*, 2010, **132**, 13645–13647.

39 (*a*) K. A. Cychosz, A. G. Wong-Foy and A. J. Matzger, *J. Am. Chem. Soc.*, 2008, **130**, 6938–6939; (*b*) K. A. Cychosz, A. G. Wong-Foy and A. J. Matzger, *J. Am. Chem. Soc.*, 2009, **131**, 14538–14543; (*c*) R. Ahmad, A. G. Wong-Foy and A. J. Matzger, *Langmuir*, 2009, **25**, 11977–11979.

40 S. Han, Y. Wei, C. Valente, I. Lagzi, J. J. Gassensmith, A. Coskun, J. F. Stoddart and B. A. Grzybowski, *J. Am. Chem. Soc.*, 2010, **132**, 16358–16361.

41 S. Horike, M. Dinca, K. Tamaki and J. R. Long, *J. Am. Chem. Soc.*, 2008, **130**, 5854–5855.

42 S. Hasegawa, S. Horike, R. Matsuda, S. Furukawa, K. Mochizuki, Y. Kinoshita and S. Kitagawa, *J. Am. Chem. Soc.*, 2007, **129**, 2607–2614.

43 (*a*) B. Gomez-Lor, E. Gutierrez-Puebla, M. Iglesias, M. A. Monge, C. Ruiz-Valero and N. Snejko, *Inorg. Chem.*, 2002, **41**, 2429–2432; (*b*) X. Zhang, F. X. Llabre′s i Xamena and A. Corma, *J. Catal.*, 2009, **265**, 155–160.

44 (*a*) M. C. Bernini, F. Gandara, M. Iglesias, N. Snejko, E. Gutierrez-Puebla, E. V. Brusau, G. E. Narda and M. A. Monge, *Chem.–Eur. J.*, 2009, **15**, 4896–4905; (*b*) F. Gandara, E. Gutierrez-Puebla, M. Iglesias, D. M. Proserpio, N. Snejko and M. A. Monge, *Chem. Mater.*, 2009, **21**, 655–661.

45 (*a*) S. H. Cho, B. Ma, S. T. Nguyen, J. T. Hupp and T. E. Albrecht-Schmitt, *Chem. Commun.*, 2006, 2563–2565; (*b*) M. H. Alkordi, Y. Liu, R. W. Larsen, J. F. Eubank and M. Eddaoudi, *J. Am. Chem. Soc.*, 2008, **130**, 12639–12641; (*c*) M. J. Ingleson, J. P. Barrio, J.-B. Guilbaud, Y. Z. Khimyak and M. J. Rosseinsky, *Chem. Commun.*, 2008, 2680–2682.

46 (*a*) Z. T. Yu, Z. L. Liao, Y. S. Jiang, G. H. Li, G. D. Li and J. S. Chen, *Chem. Commun.*, 2004, 1814–1815; (*b*) P. Mahata, G. Madras and S. Natarajan, *J. Phys. Chem. B*, 2006, **110**, 13759; (*c*) M. Alvaro, E. Carbonell, B. Ferrer, F. X. Llabrés i Xamena and H. Garcia, *Chem.–Eur. J.*, 2007, **13**, 5106–5112.

47 (*a*) P. Horcajada, S. Surblé, C. Serre, D.-Y. Hong, Y.-K. Seo, J.-S. Chang, J.-M. Grenèche, I. Margiolakid and G. Férey, *Chem. Commun.*, 2007, 2820–2822; (*b*) A. Dhakshinamoorthy, M. Alvaro and H. Garcia, *Chem.–Eur. J.*, 2010, **16**, 8530–8536.

48 S. Naito, T. Tanibe, E. Saito, T. Miyao and W. Mori, *Chem. Lett.*, 2001, 1178–1179.

49 (*a*) T. Sato, W. Mori, C. N. Kato, T. Ohmura, T. Sato, K. Yokoyama, S. Takamizawa and S. Naito, *Chem. Lett.*, 2003, **32**, 854–855; (*b*) T. Sato, W. Mori, C. N. Kato, E. Yanaoka, T. Kuribayashi, R. Ohtera and Y. Shiraishi, *J. Catal.*, 2005, **232**, 186–198; (*c*) W. Mori, T. Sato, T. Ohmura, C. N. Kato and T. Takei, *J. Solid State Chem.*, 2005, **178**, 2555–2573.

50 (*a*) R.-Q. Zou, H. Sakurai and Q. Xu, *Angew. Chem., Int. Ed.*, 2006, **45**, 2542–2546; (*b*) R.-Q. Zou, H. Sakurai, S. Han, R.-Q. Zhong and Q. Xu, *J. Am. Chem. Soc.*, 2007, **129**, 8402–8403.

51 (*a*) M. Haruta, T. Kobayashi, H. Sano and N. Yamada, *Chem. Lett.*, 1987, 405–408; (*b*) M. Haruta, N. Yamada, T. Kobayashi and S. Iijima, *J. Catal.*, 1989, **115**, 301–309.

52 (*a*) H. R. Moon, J. H. Kim and M. P. Suh, *Angew. Chem., Int. Ed.*, 2005, **44**, 1261–1265; (*b*) M. P. Suh, H. R. Moon, E. Y. Lee and S. Y. Jang, *J. Am. Chem. Soc.*, 2006, **128**, 4710–4718; (*c*) Y. E. Cheon and M. P. Suh, *Chem.–Eur. J.*, 2008, **14**, 3961–3967; (*d*) H. R. Moon and M. P. Suh, *Eur. J. Inorg. Chem.*, 2010, 3795–3803.

53 R. J. T. Houk, B. W. Jacobs, F. E. Gabaly, N. N. Chang, A. A. Talin, D. D. Graham, S. D. House, I. M. Robertson and M. D. Allendorf, *Nano Lett.*, 2009, **9**, 3413–3418.

54 A. Henschel, K. Gedrich, R. Kraehnert and S. Kaskel, *Chem. Commun.*, 2008, 4192–4194.

55 (*a*) Y. K. Hwang, D.-Y. Hong, J.-S. Chang, S. H. Jhung, Y.-K. Seo, J. Kim, A. Vimont, M. Daturi, C. Serre and G. Férey, *Angew. Chem., Int. Ed.*, 2008, **47**, 4144–4148; (*b*) M. S. Al-Shall, V. Abdelsayed, A. E. R. S. Khder, H. M. A. Hassan, H. M. El-Kaderi and T. E. Reich, *J. Mater. Chem.*, 2009, **19**, 7625–7631; (*c*) B. Yuan, Y. Pan, Y. Li, B. Yin and H. Jiang, *Angew. Chem. Int. Ed.*, 2010, **49**, 4054–4058; (*d*) Y. Pan, B. Yuan, Y. Li and D. He, *Chem. Commun.*, 2010, **46**, 2280–2282.

56 (*a*) S. Opelt, S. Türk, E. Dietzsch, A. Henschel, S. Kaskel and E. Klemm, *Catal. Commun.*, 2008, **9**, 1286–1290; (*b*) H. Liu, Y. Liu, Y. Li, Z. Tang and H. Jiang, *J. Phys. Chem. C*, 2010, **114**, 13362–13369.

57 (*a*) S. Hermes, M.-K. Schröter, R. Schmid, L. Khodeir, M. Muhler, A. Tissler, R. W. Fischer and R. A. Fischer, *Angew. Chem., Int. Ed.*, 2005, **44**, 6237–6241; (*b*) S. Hermes, D. Zacher, A. Baunemann, C. Wöll and R. A. Fischer, *Chem. Mater.*, 2007, **19**, 2168–2173; (*c*) M. Müller, O. I. Lebedev and R. A. Fischer, *J. Mater. Chem.*, 2008, **18**, 5274–5281; (*d*) F. Schröder, D. Esken, M. Cokoja, M. W. E. van den Berg, O. I. Lebedev, G. Van Tendeloo, B. Walaszek, G. Buntkovsky, H.-H. Limbach, B. Chaudret and R. A. Fischer, *J. Am. Chem. Soc.*, 2008, **130**, 6119–6130; (*e*) D. Esken, X. Zhang, O. I. Lebedev, F. Schröder and R. A. Fischer, *J. Mater. Chem.*, 2009, **19**, 1314–1319; (*f*) F. Schröder, S. Henke, X. Zhang and R. A. Fischer, *Eur. J. Inorg. Chem.*, 2009, 3131–3140; (*g*) Y. K. Park, S. B. Choi,

View Article Online

H. J. Nam, D.-Y. Jung, H. C. Ahn, K. Choi, H. Furukawa and J. Kim, *Chem. Commun.*, 2010, **46**, 3086–3088; (*h*) D. Esken, S. Turner, O. I. Lebedev, G. Van Tendeloo and R. A. Fischer, *Chem. Mater.*, 2010, **22**, 6393–6401.

58 (*a*) T. Ishida, M. Nagaoka, T. Akita and M. Haruta, *Chem.–Eur. J.*, 2008, **14**, 8456–8460; (*b*) T. Ishida, N. Kawakita, T. Akita and M. Haruta, *Gold Bull.*, 2009, **42**, 267–274; (*c*) H.-L. Jiang, B. Liu, T. Akita, M. Haruta, H. Sakurai and Q. Xu, *J. Am. Chem. Soc.*, 2009, **131**, 11302–11303; (*d*) H.-L. Jiang, Q.-P. Lin, T. Akita, B. Liu, H. Ohashi, H. Oji, T. Honma, T. Takei, M. Haruta and Q. Xu, *Chem. Eur. J.*, 2011, **17**, 78–81.

59 L. Pan, H. Liu, X. Lei, X. Huang, D. H. Olson, N. J. Turro and J. Li, *Angew. Chem., Int. Ed.*, 2003, **42**, 542–546.

60 (*a*) T. Uemura, K. Kitagawa, S. Horike, T. Kawamura, S. Kitagawa, M. Mizuno and K. Endo, *Chem. Commun.*, 2005, 5968–5970; (*b*) T. Uemura, S. Horike, K. Kitagawa, M. Mizuno, K. Endo, S. Bracco, A. Comotti, P. Sozzani, M. Nagaoka and S. Kitagawa, *J. Am. Chem. Soc.*, 2008, **130**, 6781–6788; (*c*) T. Uemura, D. Hiramatsu, Y. Kubota, M. Takata and S. Kitagawa, *Angew. Chem., Int. Ed.*, 2007, **46**, 4987–4990; (*d*) T. Uemura, R. Kitaura, Y. Ohta, M. Nagaoka and S. Kitagawa, *Angew. Chem., Int. Ed.*, 2006, **45**, 4112–4116; (*e*) T. Uemura, Y. Ono, Y. Hijikata and S. Kitagawa, *J. Am. Chem. Soc.*, 2010, **132**, 4917–4924; (*f*) T. Uemura, D. Hiramatsu, K. Yoshida, S. Isoda and S. Kitagawa, *J. Am. Chem. Soc.*, 2008, **130**, 9216–9217.

61 (*a*) B. Liu, H. Shioyama, T. Akita and Q. Xu, *J. Am. Chem. Soc.*, 2008, **130**, 5390–5391; (*b*) B. Liu, H. Shioyama, H.-L. Jiang, X.-B. Zhang and Q. Xu, *Carbon*, 2010, **48**, 456–463; (*c*) D. Yuan, J. Chen, S. Tan, N. Xia and Y. Liu, *Electrochem. Commun.*, 2009, **11**, 1191–1194; (*d*) J. Hu, H. Wang, Q. Gao and H. Guo, *Carbon*, 2010, **48**, 3599–3606; (*e*) T. Uemura, Y. Kadowaki, N. Yanai and S. Kitagawa, *Chem. Mater.*, 2009, **21**, 4096–4098.

62 R. K. Bhakta, J. L. Herberg, B. Jacobs, A. Highley, R. Behrens Jr., N. W. Ockwig, J. A. Greathouse and M. D. Allendorf, *J. Am. Chem. Soc.*, 2009, **131**, 13198–13199.

63 Z. Li, G. Zhu, G. Lu, S. Qiu and X. Yao, *J. Am. Chem. Soc.*, 2010, **132**, 1490–1491.

64 (*a*) S. Jung, W. Cho, H. J. Lee and M. Oh, *Angew. Chem., Int. Ed.*, 2009, **48**, 1459–1462; (*b*) W. Cho, Y. H. Lee, H. J. Lee and M. Oh, *Chem. Commun.*, 2009, 4756–4758.

65 (*a*) B. Liu, R.-Q. Zou, R.-Q. Zhong, S. Han, H. Shioyama, T. Yamada, G. Maruta, S. Takeda and Q. Xu, *Microporous Mesoporous Mater.*, 2008, **111**, 470–477; (*b*) B. Liu, X. B. Zhang, H. Shioyama, T. Mukai, T. Sakai and Q. Xu, *J. Power Sources*, 2010, **195**, 857–861; (*c*) B. Liu, S. Han, K. Tanaka, H. Shioyama and Q. Xu, *Bull. Chem. Soc. Jpn.*, 2009, **82**, 1052–1054.

66 H. Li, M. Eddaoudi, M. O'Keeffe and O. M. Yaghi, *Nature*, 1999, **402**, 276–279.

67 H. K. Chae, D. Y. Siberio-Pérezl, J. Kim, Y. Go, M. Eddaoudi, A. J. Matzger, M. O'Keeffe and O. M. Yaghi, *Nature*, 2004, **427**, 523–527.

68 K. Barthelet, J. Marrot, D. Riou and G. Férey, *Angew. Chem., Int. Ed.*, 2002, **41**, 281–284.

69 T. Loiseau, C. Serre, C. Huguenard, G. Fink, F. Taulelle, M. Henry, T. Bataille and G. Férey, *Chem.–Eur. J.*, 2004, **10**, 1373–1382.

70 S. S.-Y. Chui, S. M.-F. Lo, J. P. H. Charmant, A. G. Orpen and I. D. Williams, *Science*, 1999, **283**, 1148–1150.

71 (*a*) X. C. Huang, Y. Y. Lin, J. P. Zhang and X. M. Chen, *Angew. Chem., Int. Ed.*, 2006, **45**, 1557–1559; (*b*) K. S. Park, Z. Ni, A. P. Côté, J. Y. Choi, R. Huang, F. J. Uribe-Romo, H. K. Chae, M. O'Keeffe and O. M. Yaghi, *Proc. Natl. Acad. Sci. U. S. A.*, 2006, **103**, 10186–10191.

72 C. Volkringer, D. Popov, T. Loiseau, G. Férey, M. Burghammer, C. Riekel, M. Haouas and F. Taulelle, *Chem. Mater.*, 2009, **21**, 5695–5697.

Downloaded by University of Science and Technology of China on 07/05/2013 04:06:21.
Published on 02 February 2011 on http://pubs.rsc.org | doi:10.1039/C0CC05419D

 This journal is © The Royal Society of Chemistry 2011